Bioorganic Chemistry 145 (2024) 107215

Contents lists available at ScienceDirect

Bioorganic Chemistry

journal homepage: www.elsevier.com/locate/bioorg

# Discovery of a doublecortin-like kinase 1 inhibitor to prevent inflammatory responses in acute lung injury

Binhao Cai [a,b,c,1], Ying Xu [b,1], Ruixiang Luo [b,1], Kongqin Lu [d], Yuhan Wang [b], Lei Zheng [b], Yawen Zhang [b], Lina Yin [b], Linglan Tu [b], Wu Luo [c], Lulu Zheng [e], Fengzhi Zhang [b], Xinting Lv [b], Qidong Tang [c,*], Guang Liang [a,b,c,*], Lingfeng Chen [a,b,*]

[a] Department of Pharmacy and Institute of Inflammation, Zhejiang Provincial People's Hospital, Affiliated People's Hospital, Hangzhou Medical College, Hangzhou, Zhejiang 310014, China
[b] School of Pharmacy, Hangzhou Medical College, Hangzhou 310012 Zhejiang, China
[c] Chemical Biology Research Center, School of Pharmaceutical Sciences, Wenzhou Medical University, Wenzhou, Zhejiang 325035, China
[d] Schol of Basic Medicine, Inner Mongolia Medical University, Hohhot 010059, China
[e] Department of Pharmacy, Tongde Hospital of Zhejiang Province, Hangzhou, Zhejiang 310000, China

ARTICLE INFO

*Keywords:*
Doublecortin-like kinase 1
Anti-inflammatory
Drug design
Acute lung injury

ABSTRACT

Doublecortin-like kinase 1 (DCLK1) is a microtubule-associated protein kinase involved in neurogenesis and human cancer. Recent studies have revealed a novel functional role for DCLK1 in inflammatory signaling, thus positioning it as a novel target kinase for respiratory inflammatory disease treatment. In this study, we designed and synthesized a series of NVP-TAE684-based derivatives as novel anti-inflammatory agents targeting DCLK1. Bio-layer interferometry binding screening and kinase assays of the NVP-TAE684 derivatives led to the discovery of an effective DCLK1 inhibitor (a24), with an $IC_{50}$ of 179.7 nM. Compound a24 effectively inhibited lipopolysaccharide (LPS)-induced inflammation in macrophages with higher potency than the lead compound. Mechanistically, compound a24 inhibited LPS-induced inflammation by inhibiting DCLK1-mediated IKKβ phosphorylation. Furthermore, compound a24 showed *in vivo* anti-inflammatory activity in an LPS-challenged acute lung injury model. These findings suggest that compound a24 may serve as a novel candidate for the development of DCLK1 inhibitors and a potential therapeutic agent for the treatment of inflammatory diseases.

## 1. Introduction

Acute lung injury (ALI) is one of the common clinical complications commonly caused by pneumonia, sepsis, inhalation of toxicants, severe trauma, shock, or other factors [1–3]. As an inflammatory pulmonary condition, the balance of anti-inflammatory and proinflammatory cytokines governs the development of ALI [1–3]. Studies have reported increased levels of several inflammatory cytokines, including tumor necrosis factor (TNF) [4] and interleukin-6 (IL-6) [5], in both human ALI and experimental models. Although many clinical trials have attempted to inhibit the inflammatory cascade through various targets, there has been limited success in developing effective drug therapies to treat ALI [6]. Therefore, it is still challenging to develop novel and highly effective anti-inflammatory drugs for ALI treatment.

Doublecortin-like kinase 1 (DCLK1), also called KIAA0369 or DCAMKL1, is a serine/threonine kinase with two tandem doublecortin (DCX) domains and a kinase domain connected with a PEST linker (Fig. 1A) [7]. DCLK1 is involved in neurogenesis, and its expression is elevated in a wide range of human cancers, including pancreatic cancer [8,9]. Recently, our group revealed a novel function and mechanism for DCLK1 in inflammatory diseases via direct interaction with inhibitor of κB kinase β (IKKβ). Mechanistically, activated DCLK1 induces IKKβ

*Abbreviations:* ALI, Acute lung injury.; BALF, bronchoalveolar lavage fluid.; BLI, bio-layer interferometry assay.; DCLK1, doublecortin-like kinase 1.; IL-6, interleukin-6.; IKKβ, inhibitor of κB kinase β.; IκB-α, Inhibitor of κB.; LRRK2, leucine-rich repeat kinase 2.; LPS, lipopolysaccharide.; NF-κB, nuclear factor-κB.; TEA, triethylamine.; TNF, tumor necrosis factor.

* Corresponding authors at: Department of Pharmacy and Institute of Inflammation, Zhejiang Provincial People's Hospital, Affiliated People's Hospital, Hangzhou Medical College, Hangzhou, Zhejiang 310014, China (G. Liang and L. Chen).
*E-mail addresses:* tangqidongcn@126.com (Q. Tang), wzmcliangguang@163.com (G. Liang), lfchen@hmc.edu.cn (L. Chen).
[1] These authors contributed equally to this work.

https://doi.org/10.1016/j.bioorg.2024.107215
Received 24 December 2023; Received in revised form 7 February 2024; Accepted 14 February 2024
Available online 16 February 2024

phosphorylation on Ser177/181, thereby initiating the nuclear factor-κB (NF-κB) pathway (Fig. 1B) [10,11]. *In vivo*, both myeloid-specific DCLK1 knockout and pharmacological DCLK1 inhibition protect against lipopolysaccharide (LPS)-induced ALI or septic shock. Thus, DCLK1 has emerged as a novel target for developing anti-inflammatory agents.

To date, only a few small molecule inhibitors of DCLK1 have been identified, and the structural types of these compounds are limited (Fig. 2A). LRRK2-IN-1, a kinase inhibitor originally developed for Leucine-rich repeat kinase 2 (LRRK2), was the first reported compound that binds to DCLK1 ($IC_{50}$ = 2346 nM) [12,13]. Another compound, XMD8-92, was developed as a MAPK7 inhibitor but also exhibited DCLK1 inhibitory activity ($IC_{50}$ = 1982 nM) [12,14,15]. More recently, the first DCLK1 selective inhibitor, DCLK1-IN-1, has been developed, demonstrating no significant inhibitory activity against MAPK7 or LRRK2 [8,9]. Interestingly, all these inhibitors adopt a similar binding mode (type I) and share an identical benzopyrimido–diazipinone scaffold (Fig. 2A). Therefore, the discovery of a DCLK1 inhibitor with a new scaffold may advance research on DCLK1.

Previously, Lucet et al. screened a library of 400 kinase inhibitors against DCLK1, leading to the identification of NVP-TAE684, a previously described anaplastic lymphoma kinase (ALK) kinase, with an $IC_{50}$ of 1084 nM against DCLK1 (Fig. 2B) [16]. NVP-TAE684 has a novel 2,4-diarylaminopyrimidine core that differs from the benzopyrimido–diazipinone core of LRRK-IN-1 analogs (Fig. 2A), serving as a promising potential lead compound for DCLK1 inhibitor development. Based on the crystal structure of NVP-TAE684 within the DCLK1 kinase domain (Fig. 2C, PDB ID: 5JZN), the pyrimidine core (Ring A) served as the anchor point of the DCLK1 hinge region. Ring B, incorporated by the isopropylsulfonyl moiety, formed hydrophobic interactions with the DCLK1 glycine loop [13,17]. Notably, there was a weak interaction with DCLK1 at the tip of the piperidinyl-1-methylpiperazine group in NVP-TAE684, which is an attractive modification site (Fig. 2B) [13,18]. As described by Ferguson et al. [9] and evidenced by the superposition of three compounds from the co-crystal structures (Fig. 2C), a feasible approach for developing more potent and selective DCLK1 inhibitors might involve modifying the piperdinyl-1-methylpiperazine group of DCLK1 inhibitors (Fig. 2C, highlighted by the circle).

The urea group, a strong hydrogen bond acceptor and donor, is considered an important pharmacophore that plays a key role in medicinal chemistry. Some urea derivatives, such as regorafenib, glimepiride, lisuride, and zileuton, have been approved by the FDA and are used for a variety of conditions (Fig. 2D) [19]. Thus, the urea group was used as a new fragment to replace the piperidinyl group, aiming to increase the binding activity with DCLK1. In this study, two series of NVP-TAE684 derivatives bearing urea moieties were designed and synthesized (Fig. 2E). Evaluation via bio-layer interferometry assay (BLI) screening, kinase assays, and multiple cell-based assays led to the discovery of a promising candidate, **a24**. This study provides DCLK1 inhibitors as a new scaffold for use in inflammatory disease treatment.

## 2. Results

### 2.1. Structure-activity relationship study of NVP-TAE684 derivatives

Previous work has demonstrated that the kinase function of DCLK1 mediates LPS-induced inflammatory signaling in macrophages via NF-κB activation. As shown in Fig.S1, DCLK1 knockdown or NVP-TAE684 pretreatment prevented LPS-induced IκB-α degradation and significantly decreased the nuclear translocation of the P65 subunit of NF-κB. This data suggests that DCLK1 regulates LPS-induced inflammatory

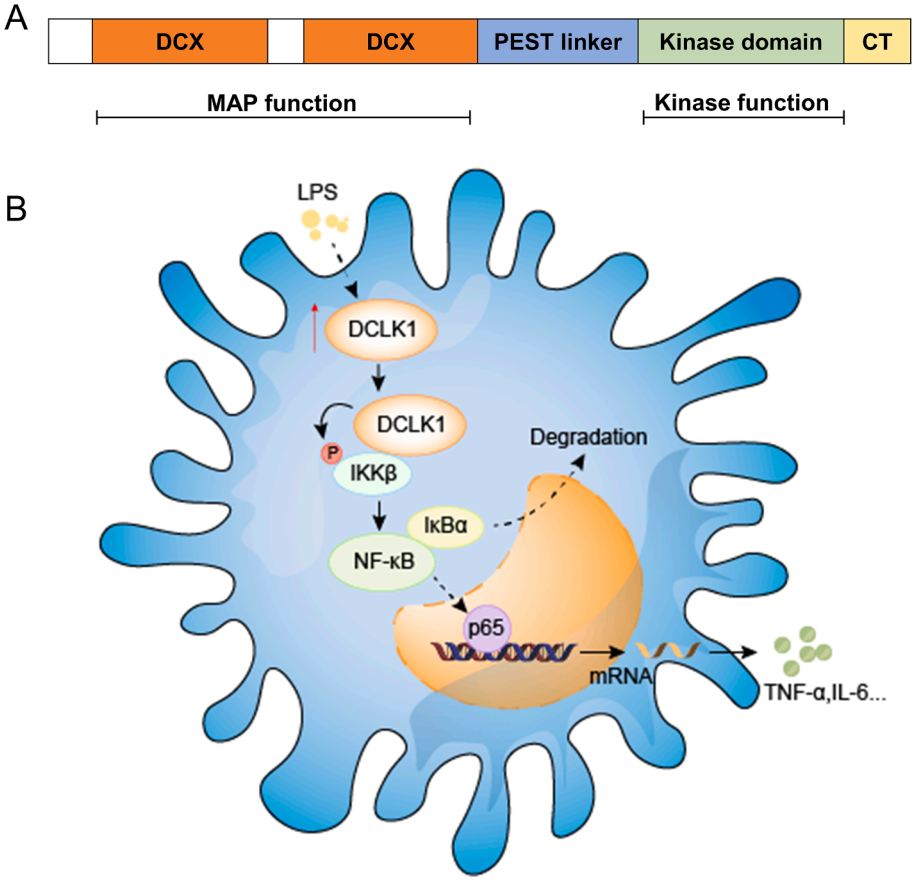


**Fig. 1.** DCLK1 is a novel regulator of inflammatory signaling. (A) Schematic presenting the constituent domains of DCLK1. (B) Doublecortin-like kinase 1 in macrophages directly binds to IKKβ and activates the NF-κB pathway to mediate LPS-induced inflammatory responses.

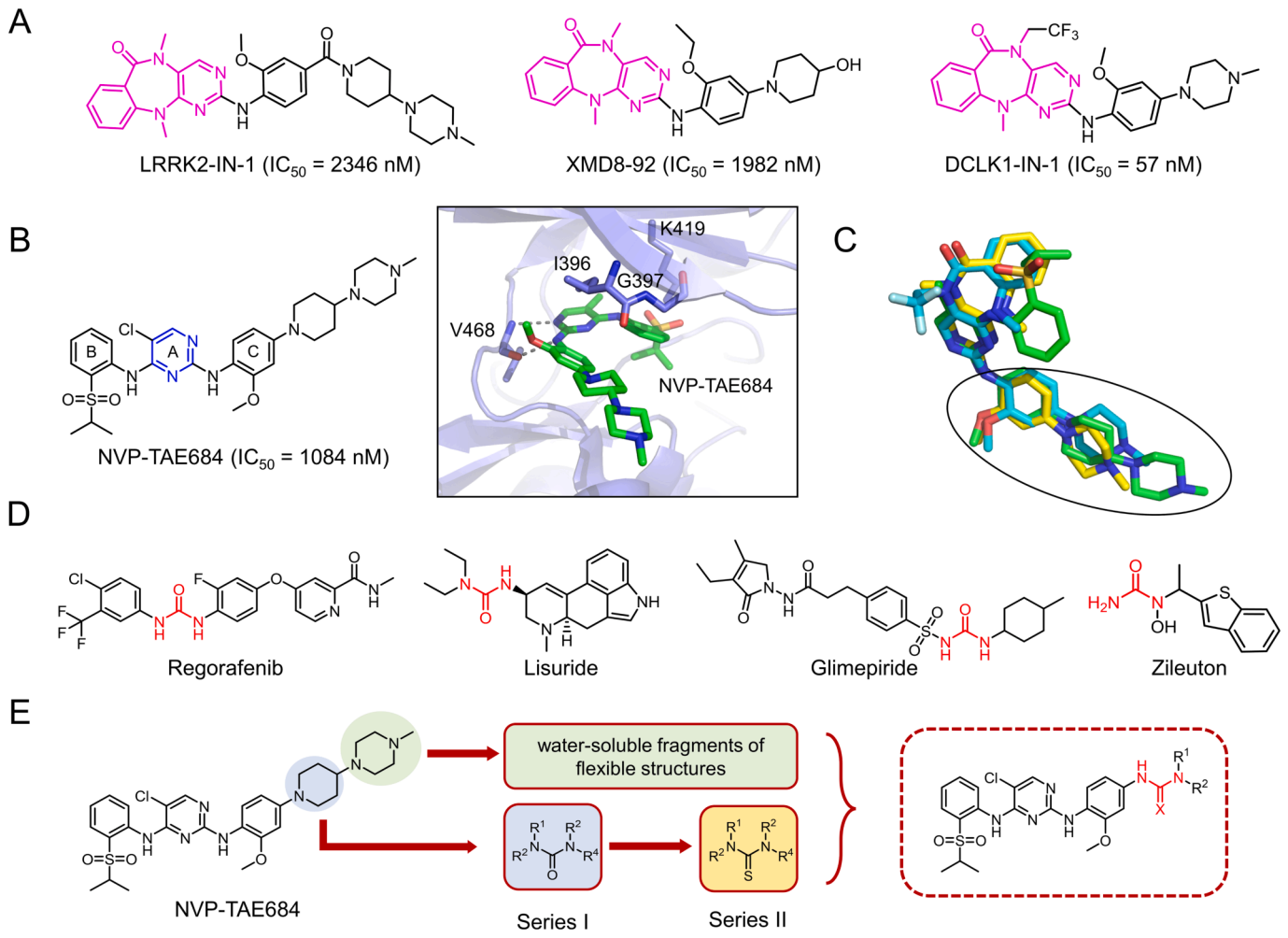


**Fig. 2.** Rationale for DCLK1 inhibitor design. (A) Structure of the reported DCLK1 inhibitors (LRRK-IN-1, XMD8-85, and DCLK1-IN-1) and their respective $IC_{50}$ values against DCLK1. (B) Structure of NVP-TAE684 and a close-up view of its interaction within the DCLK1 kinase domain (PDB ID: 5JZN). The H-bond interactions are shown as dashed lines. (C) Superposition of NVP-TAE684, XMD8-85, and DCLK1-IN-1 from the co-crystal structures. NVP-TAE684 is shown in green; XMD8-85 is shown in yellow; and DCLK1-IN-1 is shown in cyan. (D) Urea substructures are characteristic of several FDA-approved drugs. (E) Design of novel NVP-TAE684 derivatives bearing the urea moiety. (For interpretation of the references to colour in this figure legend, the reader is referred to the web version of this article.)

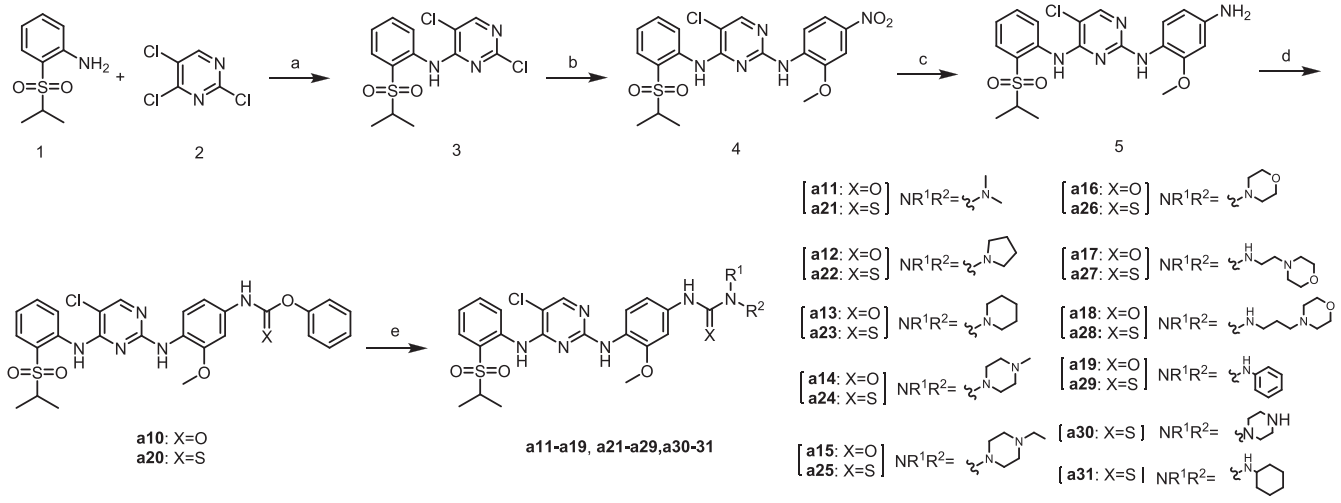


**Scheme 1.** Stepwise synthetic route of the target compounds. **Reagents and conditions:** (a) NaH, DMF, −20 ℃ to 0 ℃; (b) 2-Methoxy-4-nitroaniline, 2.5 M HCl in EtOH, 2-methoxyethanol, 120 °C, 6 h; (c) Iron powder, $NH_4Cl$, $EtOH/H_2O$ (3:1, v/v), 100 °C, reflux, 2 h; (d) Phenyl chloroformate or phenoxy thiocarbonyl chloride, DCM, 0 ℃-rt, 1 h; (e) Various substituted amines, TEA, MeCN, 0.5–2 h.

**Table 1**
BLI screening of NVP-TAE684 analogs.

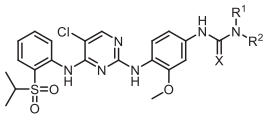

Compounds a11-a31

| Comp. | X | $R^1R^2$ | $K_D$ (μM) | Comp. | X | $R^1R^2$ | $K_D$ (μM) |
|---|---|---|---|---|---|---|---|
| NVP-TAE684 | | | 15.0 | | | | |
| a11 | O |  | 44.2 | a21 | S |  | NA |
| a12 | O |  | NA | a22 | S |  | 45.6 |
| a13 | O |  | NA | a23 | S |  | 5.70 |
| a14 | O |  | 11.4 | a24 | S |  | 2.12 |
| a15 | O | 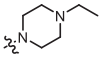 | 20.3 | a25 | S | 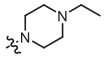 | 40.1 |
| a16 | O |  | 108.0 | a26 | S |  | NA |
| a17 | O | 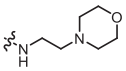 | NA | a27 | S | 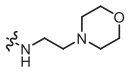 | 17.7 |
| a18 | O | 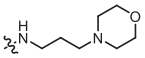 | NA | a28 | S | 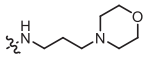 | 24.8 |
| a19 | O |  | 22.1 | a29 | S |  | 3.50 |
| | | | | a30 | S |  | 43.2 |
| | | | | a31 | S |  | 21.2 |

responses in macrophages.

As mentioned above, modifying the piperdinyl-1-methylpiperazine group of DCLK1 inhibitors may yield more potent and selective DCLK1 inhibitors (Fig. 2C). To explore this possibility, we designed two series of NVP-TAE684 derivatives bearing urea moieties. The synthetic route for all the target compounds is depicted in Scheme 1. Commercially available 2-(isopropylsulfonyl) aniline (**1**) was reacted with 2,4,5-trichloropyrimidine and sodium hydride (NaH) in *N*, *N*-dimethylformamide (DMF) to yield **3**. During hydrochloric acid (HCl) catalysis, intermediate **3** underwent nucleophilic substitution with 2-methoxy-4-nitroaniline to produce **4**, followed by reduction using an iron powder/ammonium chloride protocol, yielding the corresponding amine **5**. The amine intermediate **5** was reacted with phenyl chloroformate or phenoxy thiocarbonyl chloride to obtain the corresponding phenoxy carbonamide or O-phenyl carbamothioate derivatives (**a10** and **a20**, respectively). Finally, the target compounds (**a11-a19**, **a21-a31**) were synthesized from **a10** or **a20** by performing a nucleophilic substitution with various substituted amines in the presence of triethylamine (TEA) in methyl cyanide (MeCN).

To evaluate the interaction of the compounds with DCLK1 in vitro, the binding affinities of all synthesized NVP-TAE684 derivatives to the DCLK kinase domain (DCLK-$K_D$) were screened using the bio-layer interferometry assay (BLI). The results were presented as $K_D$ values and are summarized in Table 1 and Fig. S2. Consistent with previous reports, NVP-TAE684 directly interacted with DCLK1-$K_D$ in a dose-dependent manner, with a $K_D$ value of 15.0 μM (Table 1 and Fig. 3A). Moreover, substitution on the substructure of the urea group ($R^1R^2$) was explored. First, a dimethylamino group was introduced into this region, resulting in **a11,** which had a slightly decreased binding affinity ($K_D$ = 44.2 μM) compared to that of the lead compound NVP-TAE684 ($K_D$ = 15.0 μM). This region appeared intolerant to larger hydrophobic substituents because replacement with cyclized rings (**a12** and **a13**) led to a dramatic loss in binding potency relative to **a11**. Remarkably, the methylpiperazine group (**a14**) moderately improved the interaction with DCLK1-$K_D$ ($K_D$ = 11.4 μM). Substituting a slightly larger group, such as ethylpiperazine (**a15**), showed no improvement over **a14**. Conversely, replacement of the methylpiperazine group with various morpholine groups (**a17-a18**) largely abolished the binding affinity. Likewise, replacing the methylpiperazine ring in **a14** with an aniline moiety (compound **a19**) also slightly decreased its binding affinity for DCLK1-$K_D$. These data revealed that methylpiperazine was a key component of the pharmacophore.

Bioisosterism is a valuable approach that has been used to enhance the potency and physicochemical properties of molecules. Thiocarbonyl is a well-known bioisostere of the carbonyl groups used in medicinal chemistry. Next, we synthesized and examined a series of II NVP-TAE684 derivatives (**a21-a29**). Interestingly, most compounds exhibited increased binding activity with DCLK1-$K_D$ to varying degrees, confirming the validity of the isostere introduction. Notably, the thiourea-bearing compound (**a24**) exhibited a 5-fold lower $K_D$ value than **a14** (with $K_D$ values of 2.12 μM and 11.4 μM, respectively). A piperazine group and the cyclohexylamine group substituted compounds (**a30-a31**)

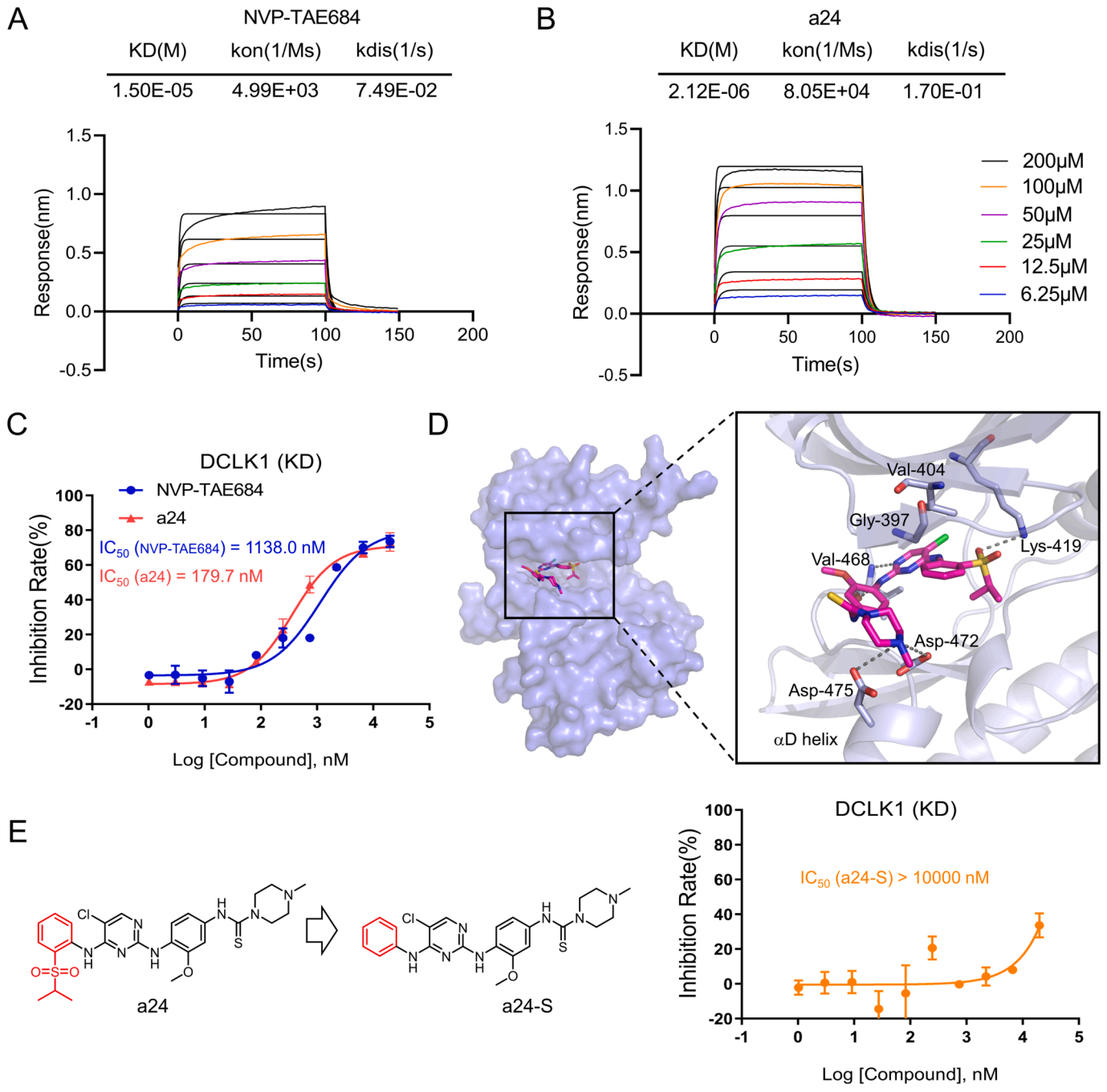


**Fig. 3.** Target validation and binding mode analysis of **a24** with DCLK1-$K_D$. (A, B) A bio-layer interferometry assay (BLI) analysis of the binding affinity between DCLK1-$K_D$ and NVP-TAE684 and **a24**. BLI shows that NVP-TAE684 and **a24** exhibit concentration-dependent binding to biotinylated-rhDCLK1 proteins bound on the SSA sensor. $K_D$, kon, and kdis values were calculated using fitted responses. (C) The inhibitory activity of NVP-TAE684 and **a24** against DCLK1-$K_D$ was measured using an ADP-Glo assay. (D) The binding mode analysis of **a24** modeled by docking with the DCLK1 kinase domain (PDB ID: 5JZN). Compound **a24** is presented as the magenta-colored stick. The interacting residues are shown as light blue-colored sticks. (E) The chemical structure of **a24** and the modified compound **a24-S**, along with the inhibitory activity of **a24-S** against DCLK1-$K_D$. (For interpretation of the references to colour in this figure legend, the reader is referred to the web version of this article.)

were further synthesized. Both substituents resulted in a dramatic loss in binding potency indicating the methylpiperazine moiety of **a24** is favored.

As shown in Fig. 3B, compound **a24** directly interacted with biotin-labeled DCLK-$K_D$ in a dose-dependent manner, with a 7-fold stronger binding affinity than that of the lead compound NVP-TAE684. A similar trend was observed for the compounds **a13, a23**, **a19**, and **a29**. These results provide evidence that a slight atomic difference could make interaction with the desired target more favorable. In summary, the $R^1R^2$ site of the compounds possessing a suitable heteroatom electronegativity and heterocycle size may be important for the interaction of the compounds with DCLK-$K_D$.

### 2.2. Target validation and binding mode analysis of a24 with DCLK1-$K_D$

The inhibitory activity of the most promising compound, **a24**, was confirmed using a kinase assay (Fig. 3C and Fig. S3). The half-maximal inhibitory concentration ($IC_{50}$) of **a24** was 179.7 nM, which was 6.3-fold

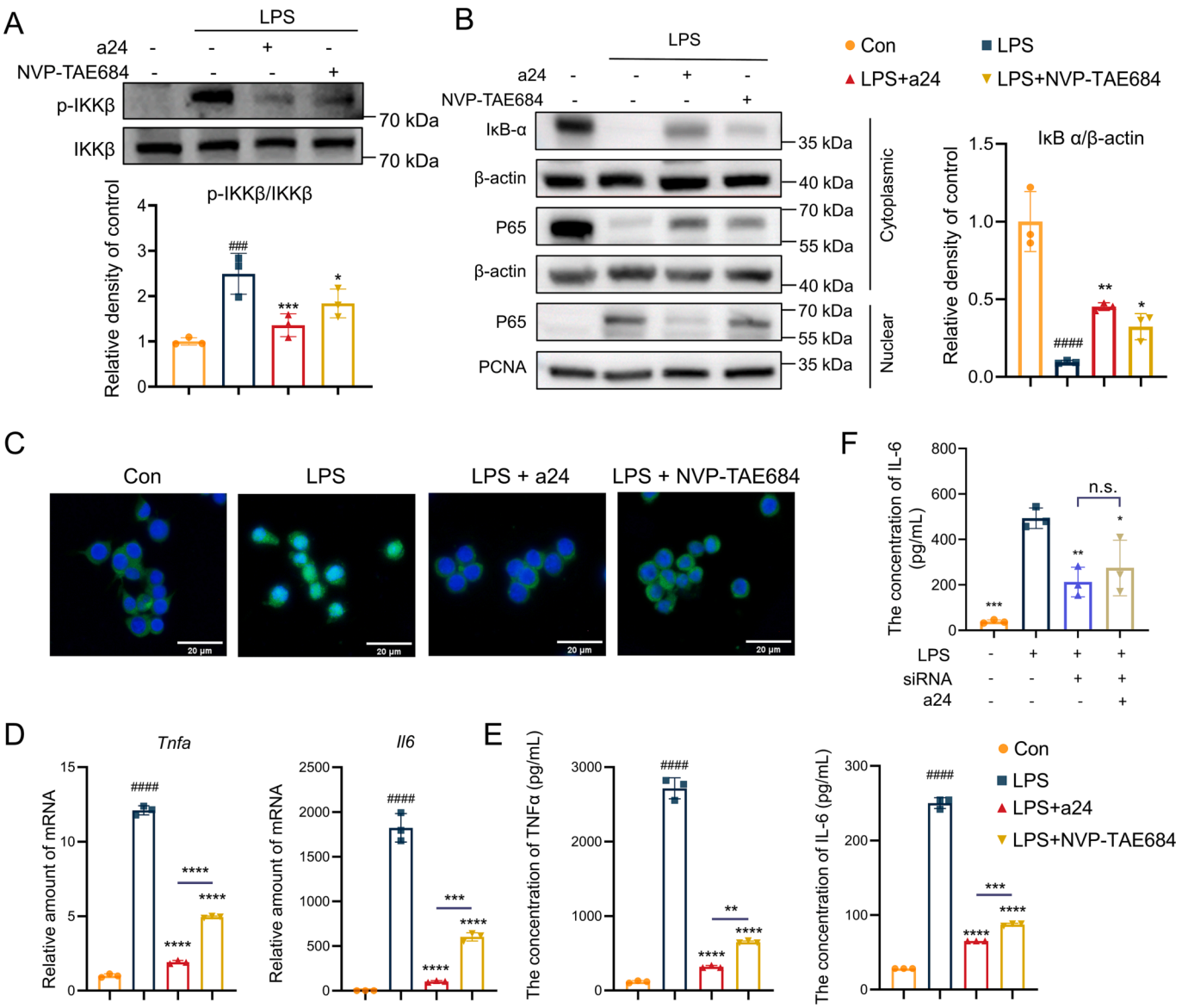


**Fig. 4.** Compound a24 inhibited LPS-induced inflammation by preventing DCLK1-IKKβ interaction. (A) RAW264.7 cells were pretreated with 10 μM a24 or NVP-TAE684for 30 min and then exposed to LPS. The phosphorylated-IKKβ levels (S177/181) were detected using western blot (WB). Quantitative analysis of the WB bands was performed. [n = 3–4; *p < 0.05, ***p < 0.001]. (B) RAW 264.7 cells were pretreated with 10 μM a24 or NVP-TAE684 for 30 min and subsequently exposed to 0.5 μg/mL LPS for 6 h. IκB-α and NF-κB P65 (cytoplasmic and nuclear fractions) protein levels were measured. β-actin and PCNA were used as loading controls for the cytoplasmic and nuclear fractions, respectively. Quantitative analysis of the western blot bands was performed using ImageJ analysis software. (C) RAW 264.7 cells were pretreated with 10 μM a24 or NVP-TAE684 for 30 min, then exposed to 0.5 μg/mL LPS for 2 h. Cells were then fixed and stained for the NF-κB P65 subunit (green), and DAPI (blue) was used for counterstaining and quantitative analysis of the fractions. Scalebar = 20 μm. (D) *Tnfa* and *Il6* mRNA levels of treated RAW 264.7 cells were determined. (E) TNF-α and IL-6 protein levels in treated RAW 264.7 cells were detected by ELISA. (F) RAW264.7 cells were transfected with DCLK1 siRNA and treated with 10 μM a24 or NVP-TAE684. Cells were then exposed to 0.5 μg/mL LPS. *Il6* mRNA levels and IL-6 protein levels were detected. [n = 3–4; *p < 0.05, **p < 0.01, ***p < 0.001, and ****p < 0.0001. ns, no significant differences]. (For interpretation of the references to colour in this figure legend, the reader is referred to the web version of this article.)

lower than that of the lead compound NVP-TAE684 ($IC_{50}$ of 1138.0 nM). We next conducted a cellular thermal shift assay (CETSA) to evaluate **a24**-DCLK1 interactions. In the CETSA assay, the ability of **a24** to increase the thermal stability of DCLK1 characterizes the target engagement of **a24**. RAW264.7 macrophages were treated with 10 μM compound **a24** for 12 h, and the collected macrophages were exposed to the temperature range. As shown in Fig. S4A, a24 pretreatment increased the soluble DCLK1 levels in macrophages by more than 3 °C compared with DMSO treatment cells, confirming that **a24** binds to DCLK1 in the cellular context.

To understand the molecular basis of the **a24**-DCLK1 interaction, a molecular docking study was performed using the crystal structure of the DCLK1 kinase domain. Docking analysis indicated that compound **a24** acts as a type I binding mode kinase inhibitor (Fig. 3D). Similar to the lead compound, NVP-TAE684, the pyrimidine core formed two hydrogen bonds with the backbone of the Val-468 residue in the kinase hinge region. The sulphonyl oxygen of the isopropylsulphonyl moiety formed a direct key polar interaction with Lys-419. Interestingly, the piperdinyl-1-methylpiperazine group of NVP-TAE684 extended into the solvent region (Fig. 2B), resulting in van der Waals interactions with the glycine loop and αC helix of DCLK1. In contrast, the introduction of a thiourea fragment in **a24** resulted in a deviation of the piperazine ring by approximately 45° compared with NVP-TAE684 (Fig. 3D). Furthermore, the N atom of the inward-turned piperazine formed two

additional hydrogen bonds with Asp-472 and Asp-475 in the αD helix of DCLK1.

To further validate the role of the isopropylsulfonyl moiety in compound **a24**, a control compound, **a24-S**, was synthesized and evaluated using a kinase assay under similar conditions (Fig. 3E). Based on the kinase assay results, removal of the isopropylsulfonyl moiety significantly abolished the DCLK1 kinase inhibition capability ($IC_{50} > 10$ μM). These results indicate that the isopropylsulfonyl group is indispensable for DCLK1 kinase inhibition. These observations are consistent with the SAR and binding mode analyses (Table 1 and Fig. 3D). The most active compound, **a24**, was selected for the subsequent biological studies.

### 2.3. Compound a24 inhibited LPS-induced inflammation by inhibiting DCLK1-mediated IKKβ phosphorylation

Previous cell-free phosphorylation studies have indicated that DCLK1 interacts with IKKβ, subsequently leading to phosphorylation at the S177/S181 site of IKKβ [11,20]. Thus, we tested the effect of **a24** on LPS-induced IKKβ phosphorylation. Western blot assays showed that **a24** treatment significantly reduced DCLK1-mediated phosphorylation of IKKβ upon LPS stimulation in RAW264.7 macrophages (Fig. 4A). IKKβ phosphorylation leads to degradation of IκB-α, thereby activating the two subunits of NF-κB and transporting them from the cytoplasm to the nucleus to initiate inflammatory cytokine transcription [21,22]. Subsequently, we evaluated IκB-α levels as an indicator of NF-κB activation in **a24-** or NVP-TAE684-treated RAW264.7 macrophage cell lysates. As shown in Fig. 4B, a24 pretreatment significantly prevented LPS-induced IκB-α degradation and decreased NF-κB P65 levels in the nucleus. Quantitative analysis indicated that **a24** exhibited stronger anti-inflammatory activity than NVP-TAE684. Immunofluorescence staining further demonstrated that upon LPS stimulation, the P65 subunit of NF-κB rapidly translocated into the nuclei in RAW264.7 cells, while **a24** treatment reduced nuclear translocation (Fig. 4C). Our results demonstrated that DCLK1 inhibition by **a24** normalizes LPS-induced interleukin-6 (IL-6) and tumor necrosis factor α (TNFα) protein levels and mRNA expression as well as cytokine production in macrophages (Fig. 4D,E). The CCK8 assay revealed that compound a24 showed no obvious toxicity against RAW264.7 at the same concentration (Fig. S5). In addition, complex of IKKβ and DCLK1 were detected by co-immunoprecipitation. Pretreatment of compound a24 inhibiting DCLK1-IKKβ interaction induced by LPS (Fig. S4B).

Although NVP-TAE684 also inhibits ALK [16], our results indicated that LPS challenge did not change *Alk* mRNA levels in macrophages (Fig. S6). In contrast, both RAW264.7 cells and mouse primary macrophages (MPMs) transcript high level of *Dclk1* gene in response to LPS, suggesting that macrophage ALK may not be involved in the inflammatory response. To further validate that the anti-inflammatory effect of the active compound **a24** in macrophages was mediated by inhibiting DCLK1 activity rather than inhibiting ALK, we evaluated **a24** in DCLK1 knockdown cells. IL-6 cytokine production was significantly suppressed after siRNA treatment compared to the control group, which was consistent with the positive role of macrophage DCLK1 in LPS-induced inflammation. Interestingly, DCLK1-depleted RAW264.7 cells were considerably less sensitive to **a24** treatment, suggesting that DCLK1 is the major anti-inflammatory target of **a24** (Fig. 4F). Collectively, these results indicate that **a24** blocks DCLK1-mediated NF-κB activation and LPS-induced inflammatory responses in macrophages.

### 2.4. The protective effect of a24 on LPS-induced ALI in mice

Recent preclinical data have provided proof-of-concept that DCLK1 is a candidate therapeutic target for the treatment of respiratory inflammatory diseases. We next investigated the pharmacokinetics (PK) profile of **a24** in mice to assess the suitability for further *in vivo* studies (Table 2). The plasma concentrations of **a24** were tested following a single-dose administration of **a24** via intravenous injection (IV, 1 mg/kg) or oral administration (20 mg/kg). As shown in Table 2, a24 showed fast absorption after PO dosing, with $C_{max}$ reached at 3.3 h. Notably, a24 is orally bioavailable with $F = 27.0$ %.

Owing to its excellent anti-inflammatory effects in RAW264.7 cells and acceptable PK profile, we assessed the therapeutic effect of **a24** in an LPS-induced ALI animal model. C57BL/6 mice were treated with 10 mg/kg of **a24** before an LPS (5 mg/kg) challenge. NVP-TAE684 was used as the positive control. As shown in Fig. 5A and B, the lung wet/dry weight ratio, an index of lung edema, was significantly decreased in the **a24**-treated group than in the control and NVP-TAE684-treated groups. The bronchoalveolar lavage fluid (BALF) of the mice was harvested following the LPS challenge. Remarkably lower cell counts demonstrated the protective effect of **a24** in the ALI mouse model (Fig. 5C). Moreover, inflammatory cytokine (e.g., TNF-α and IL-6) induction in the BALF in response to LPS was also reduced in mice treated with **a24** (Fig. 5D,E). In addition, the transcript levels of two cytokines in lung tissues were suppressed by **a24** treatment (Fig. 5F,G), with the *Tnfa* level in particular significantly lowered to the control level. Histological analyses of lung sections further showed that **a24** prevented the structural disruption of lung tissue in response to intratracheal low-dose LPS.

We also evaluated the effect of these compounds on NF-κB activity *in vivo*. Immunoblotting of mouse lung tissue samples indicated that LPS treatment reduced IκB-α levels and promoted NF-κB P65 nuclear translocation (Fig. 5H). In contrast, these indicators of NF-κB activity were significantly reduced in the **a24**-treated group. Similar to the *in vitro* studies, **a24** exhibited superior anti-inflammatory activity compared to the lead compound NVP-TAE684. To further explore whether **a24** prevents macrophage infiltration in the LPS-induced lung injury model, we performed F4/80 staining (a macrophage marker). Immunohistochemical analysis showed higher F4/80 immunoreactivity in the lung tissues obtained from LPS-challenged mice, whereas F4/80-positive macrophages decreased significantly with **a24** and NVP-TAE684 treatment (Fig. 5A). These data demonstrated that DCLK1 inhibition by compound **a24** prevents LPS-induced NF-κB activation, thus protecting against inflammation-induced lung injury.

### 2.5. The protective effect of a24 on mice sepsis model

We further evaluated the DCLK1 inhibitors in the mouse models of sepsis. The compounds NVP-TAE684 was used as positive controls. Mice were infected with *E. coli* to induce septic shock and the survival of mice was monitored. As shown in Fig. 6, mice from control group treated with *E. coli* alone died within 36 h. However, compound **a24** treated mice exhibited significantly increased survival rate compared to control or NVP-TAE684 group. These results supported previous published data that myeloid-specific DCLK1 deficient protected mice against LPS-induced septic death [11]. Our data demonstrated that DCLK1 inhibition by compound **a24** prevents LPS-induced NF-κB activation, thus protecting against inflammation-induced lung injury and sepsis.

**Table 2**
*In vivo* pharmacokinetic properties of compound a24.

| Parameter<br>Unit | $T_{1/2}$<br>h | $T_{max}$<br>h | $C_{max}$<br>ng/mL | $AUC_{(0-\infty)}$<br>h*ng/mL | $V_{ss}$<br>mL/kg | CL<br>mL/h/kg | *F*<br>% |
|---|---|---|---|---|---|---|---|
| iv (1 mg/kg) | 5.70 ± 0.87 | 0.083 ± 0.001 | 634.7 ± 134.7 | 2415.3 ± 344.4 | 2815.7 ± 120.8 | 420.19 ± 64.99 | / |
| po (20 mg/kg) | 4.58 ± 0.62 | 3.33 ± 1.15 | 1024.8 ± 175.2 | 12844.6 ± 2390.1 | / | / | 27.05 ± 4.99 |

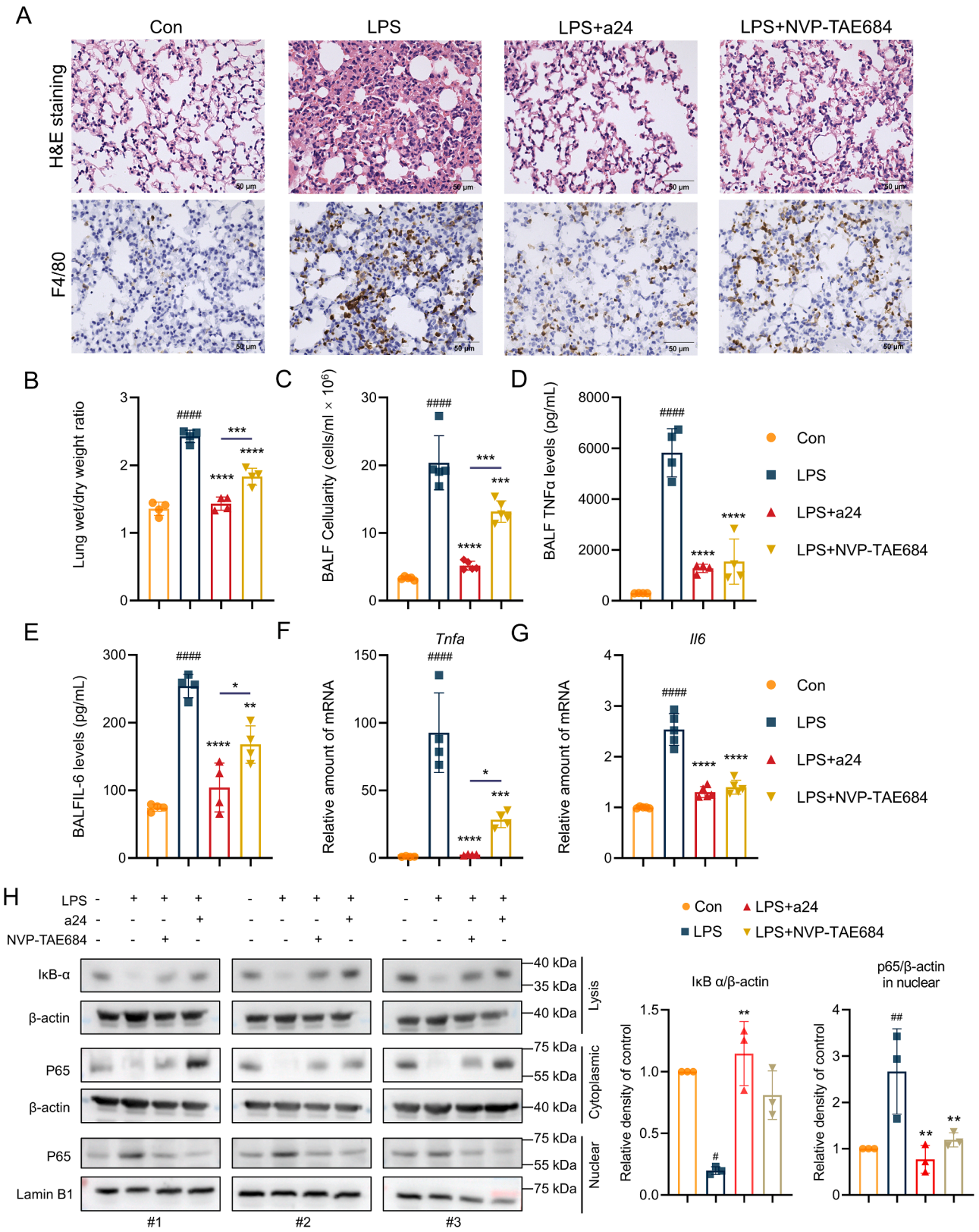


**Fig. 5.** The protective effect of **a24** on LPS-induced ALI in mice. (A) Representative H&E stained lung tissue sections. Scalebar = 50 μm; Immunohistochemical staining by F4/80 macrophage markers in LPS-induced mouse lung tissues. Immunoreactivity is depicted in brown. Scalebar = 50 μm. (B) Lung wet/dry weight ratio. (C) The total number of cells in the BALF. (D-E) TNF-α and IL-6 protein levels in BALF. (F-G) *Tnfa* and *Il6* mRNA levels in lung tissues of mice. Dunn's multiple-comparisons test was used for statistical analyses in (B-G). When compared with the LPS group, the difference was found to be statistically significant (n = 5; Mean ± SEM; *p < 0.05, **p < 0.01, ***p < 0.001, and ****p < 0.0001). (H) IκB-α and NF-κB P65 levels in lung tissue lysates. β-actin and Lamin B1 were used as loading controls, respectively. IκB-α and NF-κB P65 protein levels were measured.

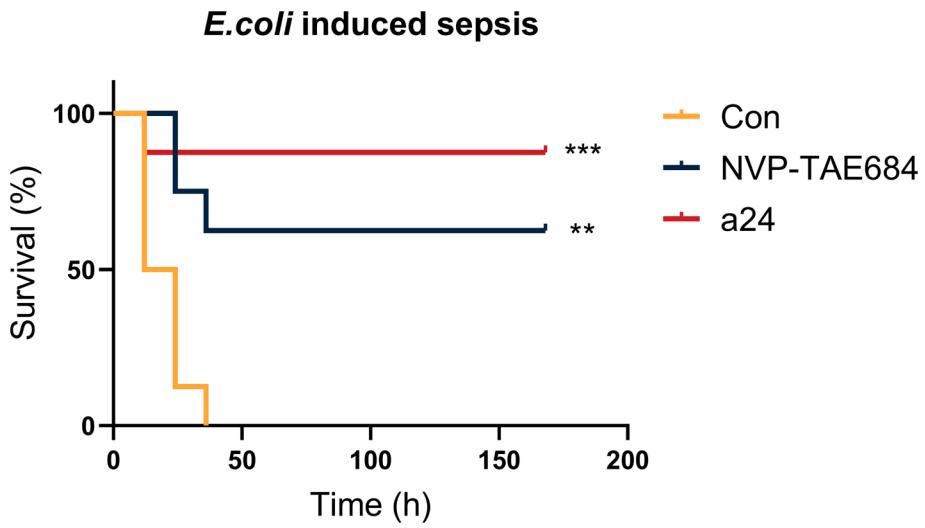


**Fig. 6.** The protective effect of a24 on mice sepsis model. C57BL/6 mice were pretreated with NVP-TAE684, a24 (10 mg/kg) or vehicle alone twice a day for one day prior to *E. coli* infection. Survival was monitored every 12 h. For all panels, Kaplan-Meier survival curves were used for analysis [n = 8 per group; **p < 0.01, ***p < 0.001].

## 3. Conclusions

Various studies have reported the potential functional role of the DCLK1 DCX domain during neuronal development, including neurogenesis and neuronal migration [23–28]. However, only a few studies have indicated the function of the DCLK1 kinase domain. DCLK1 has been found to be overexpressed in several cancers, including colon, pancreatic, and renal cell carcinoma [29–31]. Suppressing DCLK1 expression or its kinase activity resulted in decreased expression of EMT markers, which are crucial for tumor metastasis [32,33]. However, the therapeutic benefit of selectively targeting DCLK1 kinase activity in inflammation-related diseases remains unclear.

In this study, we demonstrated for the first time that the anti-inflammatory effect of NVP-TAE684 was mediated by the inhibition of DCLK1 kinase activity. Ureas have a wide range of applications in drug discovery and can increase target inhibition potency, elevate target selectivity, modify the physicochemical properties of compounds, and also assist in overcoming metabolic liability [34]. Exploring the SAR of the piperdinyl-1-methylpiperazine group in NVP-TAE684 by substituting it with thiourea moieties led to the identification of a novel derivative, **a24**. BLI and kinase assays indicated that **a24** showed a 7-fold improvement in DCLK1 binding affinity and kinase inhibition potency compared to the lead compound ($IC_{50}$ = 179.7 nM). In addition, further SAR studies clearly indicated that the isopropylsulfonyl moiety of **a24** is indispensable for DCLK1 binding.

Biological studies revealed that **a24** reduced the DCLK1-mediated phosphorylation of IKKβ upon LPS stimulation in RAW264.7 macrophages, thereby inhibiting LPS-stimulated inflammatory signaling. The DCLK1 inhibitor **a24** also exhibited a protective effect against LPS-induced ALI in mice that was superior to that of NVP-TAE684. Collectively, this study provides new lead structures and tool compounds as DCLK1 inhibitors for the development of anti-inflammatory agents.

## 4. Experimental procedures

### 4.1. Chemistry

All the target compounds were purified by column chromatography with an elution system of DCM and methanol in different ratios, and their structures were confirmed by $^1$H NMR, $^{13}$C NMR, HR-MS and LC-MS. High-resolution mass spectrometry (HRMS) (ESI) was measured using an Agilent 6520 accurate mass Q-TOF LC/MS system (1200e6520/Agilent). $^1$H and $^{13}$C NMR spectral data were recorded on a 400 MHz spectrometer (Bruker Magnet System 400′ 54 Ascend). Unless otherwise stated, all reagents and solvents were obtained from commercially available sources and used without further purification. Column chromatography was performed on 200–300 mesh silica gel.

**2,5-dichloro-N-(2-(isopropylsulfonyl)phenyl)pyrimidin-4-amine (3)**

60 % NaH (3.5 g, 75.0 mmol) was evenly dispersed in DMF (50 mL) at −20 ℃, and 2-(isopropylsulfonyl)-aniline 1 (5 g, 25.0 mmol) was added. The mixture was stirred for 30 min, and then 2,4,5-trichloropyrimidine (9.1 g, 50.0 mmol) was added slowly. The mixture was heated to room temperature and stirred for 6 h. The reaction mixture was poured into saturated ammonium chloride and extracted with EtOAc (3 × 20 mL); the organic layer was washed with brine, dried over anhydrous $MgSO_4$, concentrated, and used without further purification (yellow solid, 6.1 g, 70 % yield).

**5-chloro-N$^4$-(2-(isopropylsulfonyl)phenyl)–N$^2$-(2-methoxy-4-nitrophenyl)pyrimidine-2,4-diamine (4).** 2,5-Dichloro-N-(2-(isopropylsulfonyl)phenyl)pyrimidin-4-amine (5.0 g, 14.40 mmol, 1.0 equiv.) and 2-Methoxy-4-nitroaniline (3.64 g, 21.60 mmol, 1.5 equiv.) were dissolved in 2-methoxyethanol (40 mL). 2.5 M HCl in ethanol (10 mL) was added, and the resulting mixture was heated at 120 °C for 6 h in a sealed tube under stirring. The reaction mixture was cooled to room temperature, and the volatile components were removed *in vacuo*. The resulting residue was basified with $Na_2CO_3$ and extracted with EtOAc (3 × 20 mL), and the organic layer was washed with brine and dried over anhydrous $MgSO_4$. This was purified on a silica gel column with EA/PE (1:5, v/v) as the eluent to yield compound **2** (yellow solid, 5.8 g, 84 % yield).

**N$^2$–(4-amino-2-methoxyphenyl)-5-chloro-N$^4$-(2-(isopropylsulfonyl)phenyl)pyrimidine-2,4-diamine (5).** At ambient temperature, compound **2** (5.50 g, 11.51 mmol, 1.0 equiv.) was dissolved in an EtOH/$H_2O$ (3:1, v/v) solution (45 mL). Iron powder (3.21 g, 57.50 mmol, 5.0 equiv.) and ammonium chloride (0.92 g, 17.20 mmol, 1.5 equiv.) were then added, and the resulting mixture was heated to 100 °C and stirred for 2 h. After the reaction was complete, the mixture was cooled to room temperature and immediately filtered through a Celite filter. Next, the amount of solvent was reduced *in vacuo*, the condensed mixture was extracted with DCM, and the organic layer was washed with brine, dried over anhydrous $MgSO_4$, concentrated, and used without further purification (yellow-green solid, 5.1 g, 99 % yield).

**Phenyl (4-((5-chloro-4-((2-(isopropylsulfonyl)phenyl)amino)**

**pyrimidin-2-yl)amino)-3-methoxyphenyl)carbamate (a10).** At ambient temperature, compound **3** (5.00 g, 11.20 mmol, 1.0 equiv.) was dissolved in dry DCM (80 mL), and phenyl chloroformate (1.68 mL, 13.39 mmol, 1.2 equiv.) was slowly added dropwise in an ice bath. The reaction mixture was then heated to room temperature and stirred for 1 h. After the reaction was complete, the reaction mixture was basified with $Na_2CO_3$ until the pH reached 7 and extracted with DCM (3 × 40 mL). The organic layer was washed with brine, dried over anhydrous $MgSO_4$, concentrated, and purified by silica gel column chromatography with EA/PE (1:5, v/v) to give compound **a10** (light yellow solid, 4.85 g, 76 % yield). Analytical data for **a10**: $^1$H NMR (400 MHz, $CDCl_3$) $\delta$ 9.58 (s, 1H), 8.55 (d, $J$ = 8.4 Hz, 1H), 8.16 (d, $J$ = 8.6 Hz, 2H), 7.91 (dd, $J$ = 7.9, 1.7 Hz, 1H), 7.64 (t, 1H), 7.57 (s, 1H), 7.41 (t, $J$ = 7.8 Hz, 3H), 7.27 (m, 2H), 7.20 (dd, $J$ = 7.4, 1.6 Hz, 2H), 6.98 (s, 1H), 6.77 (dd, $J$ = 8.7, 2.3 Hz, 1H), 3.89 (s, 3H), 3.24 (p, $J$ = 6.8 Hz, 1H), 1.31 (d, $J$ = 6.9 Hz, 6H). $^{13}$C NMR (101 MHz, $CDCl_3$) $\delta$ 155.33, 155.07, 148.72, 138.35, 134.54, 134.35, 131.16, 124.74, 124.08, 123.93, 123.27, 119.50, 111.29, 103.54, 55.80, 55.57, 36.51, 15.37. ESI-MS *m/z*: 568.2 [M + H]$^+$; calcd for $C_{27}H_{26}ClN_5O_5S$: 567.1.

**O-phenyl (4-((5-chloro-4-((2-(isopropylsulfonyl)phenyl)amino) pyrimidin-2-yl)amino)-3-methoxyphenyl)carbamothioate (a20).** Phenyl chlorothionocarbonate was replaced with phenyl chloroformate to obtain target compound **a20** according to the same steps as those used for preparing compound **a10**. **a20** is difficult to store, and the crude reaction mixture was directly subjected to the next reaction without purification.

**General procedure for preparation of a11-19**

At ambient temperature, compound **a10** (0.100 g, 0.18 mmol, 1.0 equiv.) and various substituted amines (0.21 mmol, 1.2 equiv.) in MeCN (3 mL) were mixed. Following this, the reaction mixture was stirred for 0.5 h at room temperature or heated to reflux and stirred for 2 h. After the reaction was complete, the volatile components were removed *in vacuo*, and the condensed mixture was extracted with DCM (3 × 20 mL). The organic layer was washed with brine, dried over anhydrous $MgSO_4$, and concentrated. The crude product was purified by silica gel column chromatography to obtain target compounds **a11-19** at a 65–79 % yield.

**3-(4-((5-chloro-4-((2-(isopropylsulfonyl)phenyl)amino)pyrimidin-2-yl)amino)-3-methoxyphenyl)-1,1-dimethylurea (a11).** White solid; 79 % yield. Analytical data for **a11**: $^1$H NMR (400 MHz, $CDCl_3$) $\delta$ 9.53 (s, 1H), 8.56 (d, $J$ = 8.3 Hz, 1H), 8.13 (s, 1H), 8.07 (d, $J$ = 8.6 Hz, 1H), 7.90 (d, $J$ = 7.9 Hz, 1H), 7.65 (t, $J$ = 7.8 Hz, 1H), 7.50 (s, 1H), 7.36 (s, 1H), 7.25 (t, 1H), 6.67 (d, $J$ = 8.5 Hz, 1H), 6.37 (s, 1H), 3.88 (s, 3H), 3.24 (dt, $J$ = 13.6, 6.8 Hz, 1H), 3.05 (s, 6H), 1.31 (d, $J$ = 6.8 Hz, 6H). $^{13}$C NMR (101 MHz, $CDCl_3$) $\delta$ 155.46, 138.18, 134.55, 131.25, 129.49, 129.21, 125.80, 125.07, 123.51, 121.79, 121.70, 121.20, 55.82, 55.67, 15.37. ESI-LCMS: calcd for $C_{23}H_{27}ClN_6O_4S$ = 518.1, found [M + H]$^+$=519.1. ESI-HRMS: calcd for $C_{23}H_{27}ClN_6O_4S$: *m/z*: [M + H]$^+$=519.1581; found [M + H]$^+$=519.1583.

**N-(4-((5-chloro-4-((2-(isopropylsulfonyl)phenyl)amino)pyrimidin-2-yl)amino)-3-methoxyphenyl)pyrrolidine-1-carboxamide (a12).** White solid; 75 % yield. Analytical data for **a12**: $^1$H NMR (400 MHz, $CDCl_3$) $\delta$ 9.53 (s, 1H), 8.56 (d, $J$ = 8.3 Hz, 1H), 8.12 (s, 1H), 8.06 (d, $J$ = 8.4 Hz, 1H), 7.89 (d, $J$ = 7.8 Hz, 1H), 7.65 (t, $J$ = 7.7 Hz, 1H), 7.47 (d, $J$ = 21.2 Hz, 2H), 7.25 (t, $J$ = 14.0, 6.4 Hz, 1H), 6.68 (d, $J$ = 8.5 Hz, 1H), 6.25 (s, 1H), 3.88 (s, 3H), 3.47 (s, 4H), 3.24 (dt, $J$ = 13.4, 6.6 Hz, 1H), 1.98 (s, 4H), 1.30 (d, $J$ = 6.7 Hz, 6H). $^{13}$C NMR (101 MHz, $CDCl_3$) $\delta$ 155.32, 155.13, 154.12, 148.75, 138.37, 134.54, 134.49, 131.15, 124.70, 123.92, 123.85, 123.23, 119.57, 110.86, 105.74, 103.20, 55.79, 55.56, 45.82, 25.63, 15.37. ESI-LCMS: calcd for $C_{25}H_{29}ClN_6O_4S$ = 544.2, found [M + H]$^+$=545.2. ESI-HRMS: calcd for $C_{25}H_{29}ClN_6O_4S$: *m/z*: [M + H]$^+$=545.1738; found [M + H]$^+$=545.1736.

**N-(4-((5-chloro-4-((2-(isopropylsulfonyl)phenyl)amino)pyrimidin-2-yl)amino)-3-methoxyphenyl)piperidine-1-carboxamide (a13).** White solid; 76 % yield. Analytical data for **a13**: $^1$H NMR (400 MHz, $CDCl_3$) $\delta$ 9.52 (s, 1H), 8.56 (d, $J$ = 8.3 Hz, 1H), 8.13 (s, 1H), 8.07 (d, $J$ = 8.5 Hz, 1H), 7.89 (d, $J$ = 7.8 Hz, 1H), 7.64 (t, $J$ = 7.7 Hz, 1H), 7.47 (s, 1H), 7.33 (s, 1H), 7.30–7.17 (m, 1H), 6.67 (d, $J$ = 8.4 Hz, 1H), 6.51 (s, 1H), 3.87 (s, 3H), 3.46 (s, 4H), 3.24 (p, $J$ = 6.7 Hz, 1H), 1.64 (s, 6H), 1.30 (d, $J$ = 6.8 Hz, 6H). $^{13}$C NMR (101 MHz, d-DMSO) $\delta$ 159.15, 155.80, 155.35, 155.11, 151.99, 138.69, 138.57, 135.30, 131.34, 124.60, 123.98, 123.54, 123.50, 122.19, 111.42, 103.93, 55.77, 55.39, 45.11, 26.01, 24.60, 15.33. ESI-LCMS: calcd for $C_{26}H_{31}ClN_6O_4S$ = 558.2, found [M + H]$^+$=559.3. ESI-HRMS: calcd for $C_{26}H_{31}ClN_6O_4S$: *m/z*: [M + H]$^+$=559.1894; found [M + H]$^+$=559.1901.

**N-(4-((5-chloro-4-((2-(isopropylsulfonyl)phenyl)amino)pyrimidin-2-yl)amino)-3-methoxyphenyl)-4-methylpiperazine-1-carboxamide (a14).** White solid, 65 % yield. Analytical data for **a14**: $^1$H NMR (400 MHz, $CDCl_3$) $\delta$ 9.52 (s, 1H), 8.56 (d, $J$ = 8.2 Hz, 1H), 8.12 (d, $J$ = 13.8 Hz, 2H), 7.90 (d, $J$ = 7.7 Hz, 1H), 7.65 (t, $J$ = 7.5 Hz, 1H), 7.45 (s, 1H), 7.29 (s, 1H), 7.24 (t, $J$ = 7.5 Hz, 1H), 6.68 (d, $J$ = 8.3 Hz, 1H), 6.51 (s, 1H), 3.89 (s, 3H), 3.58 (s, 4H), 3.32–3.16 (p, 1H), 2.55 (s, 4H), 2.39 (s, 3H), 1.31 (d, $J$ = 6.6 Hz, 6H). $^{13}$C NMR (101 MHz, d-DMSO) $\delta$ 159.13, 155.81, 155.41, 155.13, 152.02, 138.68, 138.21, 135.30, 131.35, 124.64, 124.03, 123.57, 111.50, 104.01, 55.79, 55.38, 54.72, 43.79, 15.33. ESI-LCMS: calcd for $C_{26}H_{32}ClN_7O_4S$ = 573.1, found [M + H]$^+$=574.1. ESI-HRMS: calcd for $C_{26}H_{32}ClN_7O_4S$: *m/z*: [M + H]$^+$=574.2003; found [M + H]$^+$=574.2000.

**N-(4-((5-chloro-4-((2-(isopropylsulfonyl)phenyl)amino)pyrimidin-2-yl)amino)-3-methoxyphenyl)-4-ethylpiperazine-1-carboxamide (a15).** White solid, 67 % yield. Analytical data for **a15**: $^1$H NMR (400 MHz, $CDCl_3$) $\delta$ 9.52 (s, 1H), 8.56 (d, $J$ = 8.3 Hz, 1H), 8.18–8.03 (m, 2H), 7.90 (d, $J$ = 7.7 Hz, 1H), 7.65 (t, $J$ = 7.6 Hz, 1H), 7.44 (s, 1H), 7.30 (s, 1H), 7.27–7.22 (m, 1H), 6.68 (d, $J$ = 8.1 Hz, 1H), 6.52 (s, 1H), 3.88 (s, 3H), 3.57 (s, 4H), 3.24 (p, $J$ = 6.5 Hz, 1H), 2.54 (s, 4H), 2.50 (t, 2H), 1.31 (d, $J$ = 6.7 Hz, 6H), 1.14 (t, $J$ = 7.0 Hz, 3H). $^{13}$C NMR (101 MHz, d-DMSO) $\delta$ 159.13, 155.81, 155.43, 152.00, 138.68, 138.24, 135.30, 131.34, 124.63, 124.01, 123.57, 123.52, 122.41, 111.50, 104.01, 55.79, 55.38, 52.62, 52.02, 43.99, 15.33. ESI-LCMS: calcd for $C_{27}H_{34}ClN_7O_4S$ = 587.2, found [M + H]$^+$=588.3. ESI-HRMS: calcd for $C_{27}H_{34}ClN_7O_4S$: *m/z*: [M + H]$^+$=588.2160; found [M + H]$^+$= 588.2160.

**N-(4-((5-chloro-4-((2-(isopropylsulfonyl)phenyl)amino)pyrimidin-2-yl)amino)-3-methoxyphenyl)morpholine-4-carboxamide (a16).** White solid, 70 % yield. Analytical data for **a16**: $^1$H NMR (400 MHz, $CDCl_3$) $\delta$ 9.63 (s, 1H), 8.53 (d, $J$ = 8.3 Hz, 1H), 8.10 (s, 1H), 8.03 (d, $J$ = 7.7 Hz, 1H), 7.90 (d, $J$ = 7.6 Hz, 1H), 7.64 (t, $J$ = 7.8 Hz, 1H), 7.29 (s, 1H), 7.24 (s, 2H), 6.68 (d, $J$ = 7.8 Hz, 1H), 6.44 (s, 1H), 3.88 (s, 3H), 3.76 (t, 4H), 3.50 (t, 4H), 3.23 (p, $J$ = 6.8 Hz, 1H), 1.31 (s, 3H), 1.30 (s, 3H). $^{13}$C NMR (101 MHz, d-DMSO) $\delta$ 159.10, 155.80, 155.67, 151.98, 138.67, 138.07, 135.30, 131.34, 124.58, 124.04, 123.59, 123.55, 122.53, 111.55, 104.04, 66.49, 55.80, 55.38, 44.62, 15.33. ESI-LCMS: calcd for $C_{25}H_{29}ClN_6O_5S$ = 560.2, found [M + H]$^+$=561.2. ESI-HRMS: calcd for $C_{25}H_{29}ClN_6O_5S$: *m/z*: [M + H]$^+$=561.1609; found [M + H]$^+$= 561.1680.

**1-(4-((5-chloro-4-((2-(isopropylsulfonyl)phenyl)amino)pyrimidin-2-yl)amino)-3-methoxyphenyl)-3-(2-morpholinoethyl)urea (a17).** White solid, 71 % yield. Analytical data for **a17**: $^1$H NMR (400 MHz, $CDCl_3$) $\delta$ 9.55 (s, 1H), 8.57 (d, $J$ = 8.3 Hz, 1H), 8.12 (d, $J$ = 8.7 Hz, 2H), 7.89 (d, $J$ = 7.8 Hz, 1H), 7.63 (t, $J$ = 7.7 Hz, 1H), 7.47 (d, $J$ = 20.3 Hz, 1H), 7.42 (s, 1H), 7.29–7.16 (m, 2H), 6.73 (d, $J$ = 8.4 Hz, 1H), 5.85 (s, 1H), 3.86 (s, 3H), 3.73 (s, 4H), 3.42 (d, $J$ = 3.2 Hz, 2H), 3.31–3.18 (m, 1H), 2.61 (d, $J$ = 13.6 Hz, 6H), 1.31 (d, $J$ = 6.8 Hz, 6H). $^{13}$C NMR (101 MHz, d-DMSO) $\delta$ 159.23, 155.80, 155.76, 155.09, 152.55, 138.72, 138.52, 135.20, 131.35, 125.38, 123.94, 123.49, 123.42, 121.74, 109.52, 104.33, 102.08, 55.73, 55.39, 15.33. ESI-LCMS: calcd for $C_{27}H_{34}ClN_7O_5S$ = 603.2, found [M + H]$^+$=604.3. ESI-HRMS: calcd for $C_{27}H_{34}ClN_7O_5S$: *m/z*: [M + H]$^+$=604.2109; found [M + H]$^+$= 604.2122.

**1-(4-((5-chloro-4-((2-(isopropylsulfonyl)phenyl)amino)pyrimidin-2-yl)amino)-3-methoxyphenyl)-3-(3-morpholinopropyl) urea (a18).** White solid, 69 % yield. Analytical data for **a18**: $^1$H NMR (400 MHz, $CDCl_3$) $\delta$ 9.55 (s, 1H), 8.57 (d, $J$ = 8.4 Hz, 1H), 8.12 (t, 2H),

7.89 (d, $J$ = 7.8 Hz, 1H), 7.63 (t, $J$ = 7.7 Hz, 1H), 7.42 (s, 1H), 7.25 (dd, $J$ = 14.7, 7.0 Hz, 2H), 7.17 (s, 1H), 6.71 (d, $J$ = 8.5 Hz, 1H), 3.85 (s, 3H), 3.65 (s, 4H), 3.32 (t, $J$ = 6.1 Hz, 2H), 3.24 (p, $J$ = 6.8 Hz, 1H), 2.51–2.42 (m, 6H), 1.72 (q, 2H), 1.31 (d, $J$ = 6.8 Hz, 6H). $^{13}$C NMR (101 MHz, d-DMSO) $\delta$ 159.23, 155.78, 155.09, 152.53, 138.71, 138.54, 135.21, 131.35, 125.33, 123.93, 123.49, 123.41, 121.70, 109.57, 104.33, 102.14, 66.64, 56.35, 55.74, 55.41, 53.85, 37.94, 27.12, 15.32. ESI-LCMS: calcd for $C_{28}H_{36}ClN_7O_5S$ = 617.2, found $[M + H]^+$=618.3. ESI-HRMS: calcd for $C_{28}H_{36}ClN_7O_5S$: $m/z$: $[M + H]^+$=618.2265; found $[M + H]^+$= 618.2282.

**1-(4-((5-chloro-4-((2-(isopropylsulfonyl)phenyl)amino)pyrimidin-2-yl)amino)-3-methoxyphenyl)-3-phenylurea (a19).** White solid, 75 % yield. Analytical data for **a19**: $^1$H NMR (400 MHz, d-DMSO) $\delta$ 9.56 (s, 1H), 8.73 (s, 1H), 8.69 (s, 1H), 8.58 (s, 1H), 8.45 (s, 1H), 8.21 (s, 1H), 7.81 (dd, $J$ = 8.0, 1.7 Hz, 1H), 7.61 (t, $J$ = 7.9 Hz, 1H), 7.51–7.44 (m, 3H), 7.37 (d, $J$ = 2.2 Hz, 1H), 7.35–7.26 (m, 3H), 7.01–6.95 (m, 1H), 6.88 (dd, $J$ = 8.5, 2.3 Hz, 1H), 3.76 (s, 3H), 3.49–3.42 (m, 1H), 1.16 (d, $J$ = 6.8 Hz, 6H). $^{13}$C NMR (101 MHz, d-DMSO) $\delta$ 159.04, 155.16, 153.07, 140.16, 138.64, 137.57, 135.26, 131.38, 129.27, 124.04, 123.64, 123.54, 122.39, 122.29, 118.68, 110.13, 102.56, 55.81, 55.35, 15.32. ESI-LCMS: calcd for $C_{27}H_{27}ClN_6O_4S$ = 566.1, found $[M + H]^+$=567.2. ESI-HRMS: calcd for $C_{27}H_{27}ClN_6O_4S$: $m/z$: $[M + H]^+$=567.1581; found $[M + H]^+$= 567.1573.

**General procedure for preparation of a21-29**

Compound **a20** was replaced with compound **a10** to obtain the target compounds **a21-31** at a 65–79 % yield, following the same steps used for preparing compounds **a11-19**.

**3-(4-((5-chloro-4-((2-(isopropylsulfonyl)phenyl)amino)pyrimidin-2-yl)amino)-3-methoxyphenyl)-1,1-dimethylthiourea (a21).** Yellow solid, 75 % yield. Analytical data for **a21**: $^1$H NMR (400 MHz, d-DMSO) $\delta$ 9.55 (s, 1H), 8.99 (s, 1H), 8.58 (d, $J$ = 8.5 Hz, 1H), 8.37 (s, 1H), 8.23 (s, 1H), 7.81 (dd, $J$ = 8.0, 1.6 Hz, 1H), 7.73 (ddd, $J$ = 8.7, 7.3, 1.7 Hz, 1H), 7.57 (d, $J$ = 8.5 Hz, 1H), 7.32 (dd, $J$ = 15.2, 1.1 Hz, 1H), 7.08 (d, $J$ = 2.2 Hz, 1H), 6.85 (dd, $J$ = 8.5, 2.2 Hz, 1H), 3.74 (s, 3H), 3.44 (p, $J$ = 6.8 Hz, 1H), 3.35 (s, 6H), 1.16 (d, $J$ = 6.8 Hz, 6H). $^{13}$C NMR (101 MHz, d-DMSO) $\delta$ 186.38, 163.51, 160.00, 155.77, 143.33, 142.91, 140.36, 136.10, 129.63, 128.99, 128.52, 122.55, 114.71, 109.55, 60.78, 60.14, 46.11, 20.08. ESI-LCMS: calcd for $C_{23}H_{27}ClN_6O_3S_2$ = 534.1, found $[M + H]^+$=535.2. ESI-HRMS: calcd for $C_{23}H_{27}ClN_6O_3S_2$: $m/z$: $[M + H]^+$=535.1353; found $[M + H]^+$= 535.1348.

**N-(4-((5-chloro-4-((2-(isopropylsulfonyl)phenyl)amino)pyrimidin-2-yl)amino)-3-methoxyphenyl)pyrrolidine-1-carbothioamide (a22).** Yellow solid, 79 % yield. Analytical data for **a22**: $^1$H NMR (400 MHz, d-DMSO) $\delta$ 9.63 (s, 1H), 8.88 (s, 1H), 8.54 (s, 2H), 8.26 (s, 1H), 7.82 (dd, $J$ = 7.9, 1.7 Hz, 1H), 7.78–7.72 (m, 1H), 7.53 (d, $J$ = 8.5 Hz, 1H), 7.34 (t, $J$ = 7.7 Hz, 1H), 7.19 (s, 1H), 6.91 (dd, $J$ = 8.6, 2.3 Hz, 1H), 3.75 (s, 3H), 3.63 (s, 4H), 3.45 (p, $J$ = 6.8 Hz, 1H), 1.94 (s, 4H), 1.16 (d, $J$ = 6.8 Hz, 6H). $^{13}$C NMR (101 MHz, d-DMSO) $\delta$ 177.82, 158.14, 155.53, 151.05, 138.38, 137.91, 135.65, 131.40, 124.65, 124.49, 124.10, 123.30, 117.75, 109.99, 104.80, 56.03, 55.33, 15.32. ESI-LCMS: calcd for $C_{25}H_{29}ClN_6O_3S_2$ = 560.1, found $[M + H]^+$=561.2. ESI-HRMS: calcd for $C_{25}H_{29}ClN_6O_3S_2$: $m/z$: $[M + H]^+$=561.1509; found $[M + H]^+$= 561.1487.

**N-(4-((5-chloro-4-((2-(isopropylsulfonyl)phenyl)amino)pyrimidin-2-yl)amino)-3-methoxyphenyl)piperidine-1-carbothioamide (a23).** Yellow solid, 75 % yield. Analytical data for **a23**: $^1$H NMR (400 MHz, $CDCl_3$) $\delta$ 9.52 (s, 1H), 8.53 (dd, $J$ = 8.4, 1.1 Hz, 1H), 8.22 (d, $J$ = 8.5 Hz, 1H), 8.15 (s, 1H), 7.90 (dd, $J$ = 7.9, 1.6 Hz, 1H), 7.66 (ddd, $J$ = 8.7, 7.4, 1.7 Hz, 1H), 7.52 (s, 1H), 7.27 (d, $J$ = 7.6 Hz, 1H), 7.15 (s, 1H), 6.83 (d, $J$ = 2.3 Hz, 1H), 6.65 (dd, $J$ = 8.6, 2.3 Hz, 1H), 3.87 (s, 3H), 3.82 (t, $J$ = 5.5 Hz, 4H), 3.24 (q, $J$ = 6.8 Hz, 1H), 1.68 (s, 6H), 1.30 (d, $J$ = 6.8 Hz, 6H). $^{13}$C NMR (101 MHz, $CDCl_3$) $\delta$ 182.35, 157.36, 155.34, 155.23, 148.16, 138.27, 134.53, 134.50, 131.25, 126.41, 123.96, 123.41, 118.87, 115.94, 107.06, 55.89, 55.59, 50.43, 25.56, 24.16, 15.38. ESI-LCMS: calcd for $C_{26}H_{31}ClN_6O_3S_2$ = 574.1, found $[M + H]^+$=575.2. ESI-HRMS: calcd for $C_{26}H_{31}ClN_6O_3S_2$: $m/z$: $[M + H]^+$=575.1666; found $[M + H]^+$= 575.1660.

**N-(4-((5-chloro-4-((2-(isopropylsulfonyl)phenyl)amino)pyrimidin-2-yl)amino)-3-methoxyphenyl)-4-methylpiperazine-1-carbothioamide (a24).** Yellow solid, 70 % yield. Analytical data for **a24**: $^1$H NMR (400 MHz, $CDCl_3$) $\delta$ 9.51 (s, 1H), 8.52 (dd, 1H), 8.19 (d, $J$ = 8.6 Hz, 1H), 8.11 (s, 1H), 7.87 (dd, $J$ = 8.0, 1.7 Hz, 1H), 7.69–7.60 (m, 2H), 7.52 (s, 1H), 7.23 (dd, $J$ = 7.5, 1.1 Hz, 1H), 6.83 (d, $J$ = 2.3 Hz, 1H), 6.67 (dd, $J$ = 8.6, 2.1 Hz, 1H), 3.94 (t, $J$ = 5.1 Hz, 4H), 3.84 (s, 3H), 3.22 (p, $J$ = 6.8 Hz, 1H), 2.58 (t, 4H), 2.37 (s, 3H), 1.29 (d, $J$ = 6.9 Hz, 6H). $^{13}$C NMR (101 MHz, $CDCl_3$) $\delta$ 183.02, 157.29, 155.31, 155.13, 148.16, 138.25, 134.59, 134.12, 131.23, 126.58, 124.72, 123.83, 123.40, 118.88, 116.16, 107.20, 106.30, 55.90, 55.62, 54.14, 48.35, 45.37, 15.37. ESI-LCMS: calcd for $C_{26}H_{32}ClN_7O_3S_2$ = 589.2, found $[M + H]^+$=590.2. ESI-HRMS: calcd for $C_{26}H_{32}ClN_7O_3S_2$: $m/z$: $[M + H]^+$=590.1775; found $[M + H]^+$= 590.1778.

**N-(4-((5-chloro-4-((2-(isopropylsulfonyl)phenyl)amino)pyrimidin-2-yl)amino)-3-methoxyphenyl)-4-ethylpiperazine-1-carbothioamide (a25).** Yellow solid, 70 % yield. Analytical data for **a25**: $^1$H NMR (400 MHz, $CDCl_3$) $\delta$ 9.53 (s, 1H), 8.53 (dd, $J$ = 8.4, 1.1 Hz, 1H), 8.23 (d, $J$ = 8.6 Hz, 1H), 8.15 (s, 1H), 7.91 (d, $J$ = 8.0 Hz, 1H), 7.66 (ddd, $J$ = 8.7, 7.4, 1.7 Hz, 1H), 7.54 (s, 1H), 7.27 (d, $J$ = 7.0 Hz, 1H), 7.25–7.20 (m, 1H), 6.82 (d, $J$ = 2.4 Hz, 1H), 6.65 (dd, $J$ = 8.6, 2.3 Hz, 1H), 3.91 (t, 4H), 3.87 (s, 3H), 3.23 (p, $J$ = 6.9 Hz, 1H), 2.55 (t, $J$ = 5.1 Hz, 4H), 2.49 (q, $J$ = 7.2 Hz, 2H), 1.30 (d, $J$ = 6.9 Hz, 6H), 1.12 (t, $J$ = 7.2 Hz, 3H). $^{13}$C NMR (101 MHz, $CDCl_3$) $\delta$ 182.88, 157.31, 155.35, 155.18, 148.18, 138.24, 134.55, 134.12, 131.26, 126.60, 124.86, 123.92, 123.44, 118.86, 116.00, 107.03, 55.90, 55.62, 52.08, 48.75, 15.38, 11.75. ESI-LCMS: calcd for $C_{27}H_{34}ClN_7O_3S_2$ = 603.1, found $[M + H]^+$=604.1. ESI-HRMS: calcd for $C_{27}H_{34}ClN_7O_3S_2$: $m/z$: $[M + H]^+$=604.1931; found $[M + H]^+$= 604.1936.

**N-(4-((5-chloro-4-((2-(isopropylsulfonyl)phenyl)amino)pyrimidin-2-yl)amino)-3-methoxyphenyl)morpholine-4-carbothioamide (a26).** Yellow solid, 79 % yield. Analytical data for **a26**: $^1$H NMR (400 MHz, $CDCl_3$) $\delta$ 9.53 (s, 1H), 8.53 (d, $J$ = 8.4 Hz, 1H), 8.23 (d, $J$ = 8.6 Hz, 1H), 8.14 (s, 1H), 7.89 (dd, $J$ = 8.0, 1.6 Hz, 1H), 7.68–7.62 (m, 1H), 7.54 (s, 1H), 7.36 (s, 1H), 7.27–7.23 (m, 1H), 6.84 (d, $J$ = 2.3 Hz, 1H), 6.67 (dd, $J$ = 8.7, 2.3 Hz, 1H), 3.89–3.81 (m, 7H), 3.74 (t, $J$ = 4.8 Hz, 4H), 3.22 (p, $J$ = 6.8 Hz, 1H), 1.30 (d, $J$ = 6.9 Hz, 6H).$^{13}$C NMR (101 MHz, $CDCl_3$) $\delta$ 183.47, 157.30, 155.35, 155.16, 148.20, 138.28, 134.52, 133.92, 131.26, 126.80, 124.84, 123.86, 123.40, 118.87, 116.21, 107.20, 106.37, 66.18, 55.91, 55.63, 49.16, 29.70, 15.36. ESI-LCMS: calcd for $C_{25}H_{29}ClN_6O_4S_2$ = 576.1, found $[M + H]^+$=577.3. ESI-HRMS: calcd for $C_{25}H_{29}ClN_6O_4S_2$: $m/z$: $[M + H]^+$=577.1458; found $[M + H]^+$= 577.1451.

**1-(4-((5-chloro-4-((2-(isopropylsulfonyl)phenyl)amino)pyrimidin-2-yl)amino)-3-methoxyphenyl)-3-(2-morpholinoethyl)thiourea (a27).** Yellow solid, 74 % yield. Analytical data for **a27**: $^1$H NMR (400 MHz, $CDCl_3$) $\delta$ 9.58 (s, 1H), 8.53 (dd, $J$ = 8.4, 1.1 Hz, 1H), 8.35–8.29 (m, 1H), 8.15 (s, 1H), 7.91 (dd, $J$ = 8.0, 1.5 Hz, 1H), 7.66 (ddd, $J$ = 8.7, 7.4, 1.6 Hz, 1H), 7.57 (s, 1H), 7.29–7.24 (m, 2H), 6.88 (s, 1H), 6.81 (dd, $J$ = 8.6, 2.2 Hz, 1H), 3.88 (s, 3H), 3.83 (s, 2H), 3.71–3.63 (m, 4H), 3.23 (p, $J$ = 6.8 Hz, 1H), 2.81 (s, 2H), 2.67 (s, 4H), 1.30 (d, $J$ = 6.9 Hz, 6H). $^{13}$C NMR (101 MHz, $CDCl_3$) $\delta$ 155.36, 155.09, 148.58, 138.22, 134.52, 131.32, 124.85, 123.72, 123.46, 119.19, 117.61, 107.97, 106.72, 65.69, 56.02, 55.66, 52.95, 15.36. ESI-LCMS: calcd for $C_{27}H_{34}ClN_7O_4S_2$ = 619.2, found $[M + H]^+$=620.2. ESI-HRMS: calcd for $C_{27}H_{34}ClN_7O_4S_2$: $m/z$: $[M + H]^+$=620.1880; found $[M + H]^+$= 620.1886.

**1-(4-((5-chloro-4-((2-(isopropylsulfonyl)phenyl)amino)pyrimidin-2-yl)amino)-3-methoxyphenyl)-3-(3-morpholinopropyl) thiourea (a28).** Yellow solid, 74 % yield. Analytical data for **a28**: $^1$H NMR (400 MHz, $CDCl_3$) $\delta$ 9.58 (s, 1H), 8.53 (d, $J$ = 8.4 Hz, 1H), 8.35 (d, $J$ = 8.6 Hz, 1H), 8.15 (s, 1H), 7.91 (dd, $J$ = 8.0, 1.6 Hz, 1H), 7.69–7.61 (m, 1H), 7.56 (s, 1H), 7.28 (d, $J$ = 7.6 Hz, 1H), 7.07 (d, $J$ = 5.4 Hz, 1H), 6.84–6.71 (m, 2H), 3.88 (s, 3H), 3.74 (s, 2H), 3.39 (s, 4H), 3.23 (p, $J$ = 6.8 Hz, 1H), 2.41 (t, $J$ = 6.3 Hz, 2H), 2.33 (t, $J$ = 4.7 Hz, 4H), 1.77 (p, $J$

= 6.3 Hz, 2H), 1.30 (d, $J$ = 6.8 Hz, 6H). $^{13}$C NMR (101 MHz, $CDCl_3$) $\delta$ 157.14, 155.38, 155.12, 138.22, 134.44, 131.35, 124.95, 123.68, 123.48, 66.25, 56.01, 55.63, 53.61, 15.36, 1.02. ESI-LCMS: calcd for $C_{28}H_{36}ClN_7O_4S_2$ = 633.2, found $[M + H]^+$=634.3. ESI-HRMS: calcd for $C_{28}H_{36}ClN_7O_4S_2$: *m/z*: $[M + H]^+$=634.2037; found $[M + H]^+$= 634.2053.

**1-(4-((5-chloro-4-((2-(isopropylsulfonyl)phenyl)amino)pyrimidin-2-yl)amino)-3-methoxyphenyl)-3-phenylthiourea (a29).** Yellow solid, 75 % yield. Analytical data for **a29**: $^1$H NMR (400 MHz, $CDCl_3$) $\delta$ 9.62 (s, 1H), 8.50 (d, $J$ = 8.3 Hz, 1H), 8.27 (d, $J$ = 8.6 Hz, 1H), 8.15 (s, 1H), 7.96 (d, $J$ = 7.6 Hz, 1H), 7.90 (dd, $J$ = 7.9, 1.6 Hz, 1H), 7.74–7.60 (m, 2H), 7.41 (d, $J$ = 4.3 Hz, 4H), 7.29–7.25 (m, 2H), 7.03 (s, 1H), 6.84 (dd, $J$ = 8.5, 2.2 Hz, 1H), 5.29 (s, 1H), 3.89 (s, 3H), 3.22 (p, $J$ = 6.9 Hz, 1H), 1.30 (d, $J$ = 6.8 Hz, 6H). $^{13}$C NMR (101 MHz, $CDCl_3$) $\delta$ 156.96, 155.48, 154.46, 148.64, 138.06, 134.55, 131.33, 129.52, 126.97, 125.18, 125.03, 123.87, 123.68, 119.30, 117.75, 108.24, 56.04, 55.70, 15.37. ESI-LCMS: calcd for $C_{27}H_{27}ClN_6O_3S_2$ = 582.1, found $[M + H]^+$=583.3. ESI-HRMS: calcd for $C_{27}H_{27}ClN_6O_3S_2$: *m/z*: $[M + H]^+$=583.1353; found $[M + H]^+$=583.1343.

**N-(4-((5-chloro-4-((2-(isopropylsulfonyl)phenyl)amino)pyrimidin-2-yl)amino)-3-methoxyphenyl)piperazine-1-carbothioamide (a30).** Yellow solid, 65 % yield. Analytical data for **a30:** $^1$H NMR (400 MHz, d-DMSO) $\delta$ 9.55 (s, 1H), 9.27 (s, 1H), 8.58 (d, $J$ = 8.4 Hz, 1H), 8.39 (s, 1H), 8.23 (s, 1H), 7.81 (dd, $J$ = 8.0, 1.7 Hz, 1H), 7.78 – 7.67 (m, 1H), 7.56 (d, $J$ = 8.5 Hz, 1H), 7.32 (t, $J$ = 7.6 Hz, 1H), 7.05 (d, $J$ = 2.2 Hz, 1H), 6.82 (dd, $J$ = 8.5, 2.2 Hz, 1H), 3.85 (t, $J$ = 4.9 Hz, 4H), 3.74 (s, 3H), 2.79 (t, $J$ = 4.9 Hz, 4H), 1.22 (s, 1H), 1.16 (d, $J$ = 6.7 Hz, 6H). $^{13}$C NMR (101 MHz, d-DMSO) $\delta$ 181.68, 158.81, 155.80, 155.25, 151.15, 138.61, 138.15, 135.62, 131.39, 124.80, 124.23, 123.72, 123.39, 117.30, 109.45, 104.80, 56.07, 55.39, 49.52, 45.71, 29.53, 15.37. ESI-LCMS: calcd for $C_{25}H_{30}ClN_7O_3S_2$ = 575.1, found $[M + H]^+$=576.2. ESI-HRMS: calcd for $C_{27}H_{27}ClN_6O_3S_2$: *m/z*: $[M + H]^+$=576.1618; found $[M + H]^+$=576.1620.

**1-(4-((5-chloro-4-((2-(isopropylsulfonyl)phenyl)amino)pyrimidin-2-yl)amino)-3-methoxyphenyl)-3-cyclohexylthiourea (a31).** Yellow solid,68 % yield. Analytical data for **a31:** $^1$H NMR (400 MHz, d-DMSO) $\delta$ 9.55 (s, 1H), 9.37 (s, 1H), 8.58 (d, $J$ = 8.5 Hz, 1H), 8.40 (s, 1H), 8.23 (s, 1H), 7.81 (dd, $J$ = 8.0, 1.6 Hz, 1H), 7.74 – 7.67 (m, 1H), 7.57 (d, $J$ = 8.4 Hz, 2H), 7.35 – 7.28 (m, 2H), 6.87 (dd, $J$ = 8.5, 2.2 Hz, 1H), 4.12 (s, 1H), 3.75 (s, 3H), 3.44 (p, $J$ = 6.7 Hz, 1H), 1.91 (d, $J$ = 10.7 Hz, 2H), 1.68 (dd, $J$ = 9.3, 4.1 Hz, 2H), 1.56 (dd, $J$ = 11.1, 6.0 Hz, 1H), 1.28 (d, $J$ = 10.0 Hz, 3H), 1.25 – 1.21 (m, 2H), 1.16 (d, $J$ = 6.8 Hz, 6H). $^{13}$C NMR (101 MHz, d-DMSO) $\delta$ 179.46, 158.81, 155.79, 155.22, 151.50, 138.61, 136.47, 135.51, 131.40, 124.51, 123.71, 104.82, 56.01, 55.39, 32.37, 25.67, 25.07, 15.37. ESI-LCMS: calcd for $C_{27}H_{33}ClN_6O_3S_2$ = 588.1, found $[M + H]^+$=589.2. ESI-HRMS: calcd for $C_{27}H_{27}ClN_6O_3S_2$: *m/z*: $[M + H]^+$=589.1822; found $[M + H]^+$=589.1825.

**N-(4-((5-chloro-4-(phenylamino)pyrimidin-2-yl)amino)-3-methoxyphenyl)-4-methylpiperazine-1-carboxamide (a24-S).** Yellow solid, 73 % yield. Analytical data for **a24-S**: $^1$H NMR (400 MHz, $CDCl_3$) $\delta$ 8.23 (d, $J$ = 8.7 Hz, 1H), 8.05 (s, 1H), 7.60–7.54 (m, 2H), 7.50 (s, 1H), 7.44–7.35 (m, 3H), 7.20–7.15 (m, 1H), 7.07 (s, 1H), 6.76 (d, $J$ = 2.3 Hz, 1H), 6.57 (dd, $J$ = 8.7, 2.3 Hz, 1H), 3.87–3.81 (m, 7H), 2.44 (t, $J$ = 5.2 Hz, 4H), 2.30 (s, 3H). $^{13}$C NMR (101 MHz, $CDCl_3$) $\delta$ 183.13, 157.53, 155.83, 154.26, 147.97, 137.72, 133.81, 128.93, 126.82, 124.61, 122.31, 118.76, 115.65, 106.60, 105.02, 67.10, 55.85, 54.38, 49.09, 45.79. ESI-LCMS: calcd for $C_{23}H_{26}ClN_7O_2$ = 483.1, found $[M + H]^+$=483.7. ESI-HRMS: calcd for $C_{23}H_{26}ClN_7O_2$: *m/z*: $[M + H]^+$=484.1686; found $[M + H]^+$=484.1692.

### 4.2. Cell culture and transfection

The mouse macrophage RAW264.7 cell lines were kindly provided by the Cell Bank, Chinese Academy of Sciences. The cells were cultured in Dulbecco's modified Eagle's medium (DMEM) (Cat. BC-M−005, Bio-Channel) containing 10 % FBS (Cat. BC-SE-FBS07, Bio-Channel) and 1 % penicillin/streptomycin (Cat. No. BL505A, Biosharp) at 37 ℃ with 5 % $CO_2$. We transfected cells with targeting siRNA (mouse DCLK1 sequence: 5-GCUGGCGUGAUCACUUAUATT-3) to silence DCLK1 in RAW264.7 cells. Transfections were performed using jetPRIME® (Polyplus).

### 4.3. Bio-layer interferometry binding assays

Binding kinetic measurements were performed using bio-layer interferometry on a FortéBio Octet Red 96 instrument as previous described [35]. Purified kinase-active DCLK1 (kindly provided by Wenzhou Medical University) was biotinylated using a Biotinylation Kit (GENEMORE, #G-MM-IGT) following the manufacturer's instructions. The biotin-labeled DCLK1 protein was loaded onto super streptavidin (SSA) sensors (#18–5057, Octet) with 200 μL 25 mM HEPES, 150 mM NaCl, and 0.02 % (v/v) Tween-20 as running buffer. After equilibrium was reached, association and dissociation measurements were performed using serial dilutions of the novel NVP-TAE684 derivatives and NVP-TAE684 (6.25, 12.5, 25, 50, 100, and 200 μM). Equilibrium constant ($K_D$) values were assessed using FortéBio Data Analysis software.

### 4.4. Kinase assay

The ATPase activity of DCLK1 was measured using an ADP-Glo Kinase Assay. Reactions were carried out in 50 μL reaction buffer in the 384-well plates (#6007680, PerkinElmer): 40 mM Tris-HCl pH = 7.5, 20 mM $MgCl_2$ (M1028, Sigma), 0.1 mg/ml BSA and 50 μM DTT. The final concentrations of different components were 4.5 ng/μL purified DCLK1 protein, 10 μM ATP (#V915B, Promega) and 0.2 μg/μL Autocamtide-2tide (PE8515, GenScript). The tested compounds at different concentrations were added to the mixture and incubated at 25 °C for 60 min. ADP-Glo™ reagent (#V912B, Promega) was added to each reaction well and incubated for 40 min. Next, 10 μL kinase detection reagent (#V913B, Promega) was added to the wells and incubated for 30 min. Finally, the luminescence level was measured on the plate reader (Ensight, PerkinElmer). Results of validation and optimization of DCLK1 ADP-Glo kinase assay was provided in the supplementary data Fig. S3.

### 4.5. Molecular docking simulation of NVP-TAE684, a24, and a14 with DCLK1

Molecular modeling was performed using modules from the Schrödinger Small Molecular Drug Discovery Suite (Maestro) [36]. The X-ray crystal structure of DCLK1 (PDB ID: 5JZN) was imported from the PDB and prepared using the Protein Preparation Wizard in Maestro to optimize the downloaded proteins by removing all non-bonded heteroatoms and water molecules and adding hydrogen atoms. The charge state and lowest-energy conformation of the target compound were calculated using the LigPrep module. Docking was performed in a confined grid built 20 Å around the ATP binding site using Receptor Grid Generation and simulated using the extra precision setting in Glide.

### 4.6. Detection of TNF-α and IL-6 secretion

Culture medium and bronchoalveolar lavage fluid (BALF) collected from each mouse group were analyzed to detect TNF-α (Cat. #88–7064, ThermoFisher) and IL-6 (Cat. #88–7064, ThermoFisher) by ELISA following the manufacturer's instructions as previous described [37].

### 4.7. RNA Extraction and Real-Time PCR

The mRNA from RAW264.7 cells and lung tissues was determined using standard real-time quantitative PCR (qPCR). AG RNAex Pro RNA Extraction Reagent (Cat. #AG21101, Accurate Biotechnology) and the SteadyPure Universal RNA Extraction Kit (Cat. AG21024, Accurate Biotechnology) were used to isolate total RNA according to the

manufacturer's instructions, and the RNA concentration was determined using a NanoDrop 2000 spectrophotometer (ThermoFisher). The cDNA was synthesized using the Evo M-MLV Mix Kit with gDNA Clean for qPCR (Cat. AG11728, Accurate Biotechnology) according to the manufacturer's protocol. Gene expression levels were measured by relative quantification using the SYBR Green Premix Pro Taq HS qPCR Kit (Cat. AG11733; Accurate Biotechnology). Quantitative PCR (qPCR) amplification was performed using a CFX Connect™ Real-Time system (Bio-Rad). The $2^{-\Delta\Delta Ct}$ method was used to analyze the relative expression levels.

Mouse TNF-α forward: Forward Primer (5′-3′): TGATCCGCGACGTGGAA; Reverse Primer (5′-3′): ACCGCCTGGAGTTCTGGAA

Mouse IL-6 forward: Forward Primer (5′-3′): GAGGATACCACTCCCAACAGACC; Reverse Primer (5′-3′): AAGTGCATCATCGTTGTTCATACA

Mouse GAPDH forward: Forward Primer (5′-3′): GGAGCGAGATCCCTCCAAAAT; Reverse Primer (5′-3′): GGCTGTTGTCATACTTCTCATGG.

### 4.8. Western blot assay

Proteins were isolated from cells using lysate and centrifuged at 12,000 r/min for 10 min at 4 ℃. Following this, the supernatant was removed, and the concentration of each sample was detected using the BCA method and normalized to the same protein concentration. The protein was denatured at 100 ℃ for 10 min after diluting it with 5X protein loading buffer. Samples were separated by SDS-PAGE, transferred to polyvinylidene difluoride (PVDF) membranes in transfer buffer, and incubated overnight at 4 °C with target antibodies diluted in 5 % BSA in phosphate buffered saline Tween (PBST). An enhanced chemiluminescence reagent (NcmECL Ultra; Cat. No. P10300A; NCM Biotech) was used to visualize the antibodies in the Vilber Fusion FX system.

The following primary antibodies were used: anti-GAPDH (1:50000, Cat. ET1601-4), anti-β-actin (1:5000, Cat. R1207-1), anti-PCNA (1:1000, Cat. ET1605-38), anti-lamin B1 (1:1000, Cat. ET1606-27), IKKβ (Cat. R1706-13), IκB-α (Cat. ET1603-6), NF-κB P65 (Cat. ET1603-12), and DCLK1 (Cat. ET1704-10) antibodies, purchased from HUABIO. The anti-p-IKKβ (Tyr199) (Cat. AF3010) antibody was purchased from Affinity Biosciences (San Jose, CA, USA).

### 4.9. Co-immunoprecipitation

For co-immunoprecipitation assays, HEK-293 T cells were transfected with 3X Flag-DCLK1 plasmids (MiaoLingPlasmid). After transfection, the cells were treated with DMSO or the test compound overnight and then with LPS (Cat. No. P5552, Beyotime Biotechnology) at 50 ng/mL for 6 h. The medium was immediately removed, and co-immunoprecipitation assays were performed using a Flag-tag Protein IP Assay Kit with agarose gel (Cat. No. P2202, Beyotime Biotechnology) based on our previous published protocol [11].

### 4.10. Immunofluorescence analysis

To assess NF-κB activation, staining for NF-κB P65 translocation in the cells was performed. RAW264.7 cells were fixed with 2 % formaldehyde in PBS for 2 min, permeabilized with 0.5 % Triton X-100 in PBS for 10 min and blocked with 5 % BSA in PBS for 1 h. Fixed cells were incubated with an anti-NF-κB P65 antibody (1:100) overnight. After washing thrice with PBS, the cells were stained with Alexa Fluor 488-conjugated secondary antibodies (Cat. No. A0423, Beyotime Biotechnology) for 1 h and DAPI (Cat. No. C1002, Beyotime Biotechnology) for 10 min [11].

### 4.11. Cellular thermal shift assay

RAW264.7 cells were treated with DMSO or tested compounds overnight. Macrophage cells were collected and washed with PBS twice. Then, collected cells were aliquoted in PCR tubes and were and incubated in a PCR machine for 3 min in a temperature gradient as indicated. After the heating, tubes were incubated at 25 ℃ for another 3 min. Samples were then frozen and thawed for three times, and centrifuged for 20 min at 4 ℃. The collected supernatant was analyzed by western blotting using DCLK1 antibody.

### 4.12. Animal model of acute lung injury (ALI) and treatment

C57BL/6 mice (20 ± 2 g) were obtained from the Hangzhou Medical College Experimental Animal Center (Hangzhou, China). All animals were housed at a controlled room temperature (22 ± 1 °C), with a 12:12-h light–dark cycle, and fed a standard rodent diet and water. All animals received humane care according to the institutional animal care guidelines approved by the Experimental Animal Ethics Committee of Hangzhou Medical College. The mice were randomly divided into four groups (n = 7): control (Con), LPS-induced ALI (LPS; 5 mg/kg), LPS-induced ALI treated with 10 mg/kg NVP-TAE684 (LPS + NVP-TAE684), and LPS-induced ALI treated with 10 mg/kg **a24** (LPS + **a24**).

NVP-TAE684 and **a24** were dissolved in 0.5 % sodium carboxymethyl cellulose (CMC-Na) and administered intragastrically at 200 μL/20 g body weight; the control and LPS groups received the same volume of vehicle. After treatment with the vehicle, NVP-TAE684, or a24 for 3 days, on the fourth day, after intragastric administration for 1 h, the mice were challenged with 5 mg/kg LPS through intratracheal instillation. The mice were sacrificed after 6 h, and testing samples, including bronchoalveolar lavage fluid (BALF) and lung tissue samples, were collected.

The collected BALF was centrifuged at 1000 rpm for 10 min at 4 °C, and protein concentration and cytokine levels (TNF-α, IL-6) in the supernatant were measured. The cell particles were resuspended in 50 μL PBS, and the total number of cells was counted.

The middle lobe of the right lung was cut, and the wet weight was recorded. The lung tissue was placed in a constant-temperature oven at 65 °C for 72 h to obtain the dry weight. Finally, the wet/dry weight ratio of the lung tissue was calculated as an indicator of pulmonary edema.

### 4.13. Immunohistochemical determination

The lung tissues were immobilized in 4 % paraformaldehyde for 48 h, dehydrated using a graded alcohol series, and embedded in paraffin. Paraffin-embedded sections (5 μm) were processed for immunohistochemical staining (H&E staining), evaluated using light microscopy, and quantitative analysis was performed using ImageJ software.

Paraffin-embedded sections were deparaffinized and rehydrated, and antigens were recovered by boiling in citrate buffer (pH 6.0) for 10 min. Endogenous peroxidase activity was blocked using 3 % hydrogen peroxide. Afterwards, they were incubated with 5 % BSA for 1 h and then incubated with F4/80 primary antibody for 12 h on a shaker at 4 °C. HRP-conjugated secondary antibodies were incubated for 15 min, developed with DAB chromogen, counterstained with hematoxylin, and observed under an inverted fluorescent microscope.

### 4.14. E. Coli-induced sepsis model

Viable *E. coli* in 0.2 mL PBS ($2 \times 10^9$ CFU/mouse) were injected into the peritoneal cavity of 8 weeks old male C57BL/6 mice. To test the pharmacological effects of DCLK1 inhibitors in these models, 8 weeks old male C57BL/6 mice were pre-treated with 20 mg/kg NVP-TAE684, DCLK1-IN-1, a24 or vehicle (5 % DMSO, 30 % PEG-400 and 65 % saline) through orogastric gavage injections twice a day for three days before *E. coli* injection. After the injection, mice received the compounds or

vehicle treatment at a frequency of twice a day until the mice died or the experiment ended on the sixth day. The survival of mice was monitored during the experiments [11,20].

### 4.15. Statistical analysis

All data were obtained from at least three independent replicates and calculated as the mean ± standard error (mean ± SEM). Statistical analyses were performed using the GraphPad Prism 8.0 software (GraphPad, San Diego, CA, USA). Comparisons between the two groups were performed using a two-tailed unpaired Student's *t*-test. One-way ANOVA followed by Dunnett's post-hoc test was used to compare data from more than two groups. Statistical significance was set at $p < 0.05$. Post-tests were run only if F achieved $p < 0.05$ and there was no significant variance in homogeneity.

## Author contributions

L.C., G.L., conceived and proposed this project. B.C., Y.W., K.L., and Q.T., synthesized the target compounds. Y.X., R.L., L.T., L.Z., F.Z. and W. L. completed drug screening and cell-based studies. L.Z. completed the molecular docking study. B.C., R.L., Y.Z. and X.L. participated in the *in vivo* study. Y.Z., L.Y., L.T., L.Z. F.Z. and X.L. contributed to processing the data and revising of the manuscript. L.Z. conducted molecular docking. L.C. wrote the manuscript with input from all authors.

## CRediT authorship contribution statement

**Binhao Cai:** Validation, Investigation, Data curation. **Ying Xu:** Validation, Methodology, Investigation, Data curation. **Ruixiang Luo:** Validation, Conceptualization. **Kongqin Lu:** Writing – review & editing, Data curation. **Yuhan Wang:** Investigation. **Lei Zheng:** Writing – review & editing, Investigation. **Yawen Zhang:** Writing – review & editing, Investigation. **Lina Yin:** Writing – review & editing, Investigation. **Linglan Tu:** Methodology, Investigation. **Wu Luo:** Investigation. **Lulu Zheng:** Writing – review & editing, Investigation. **Fengzhi Zhang:** Writing – review & editing, Supervision. **Xinting Lv:** Investigation. **Qidong Tang:** Investigation. **Guang Liang:** Writing – review & editing, Supervision. **Lingfeng Chen:** Writing – review & editing, Writing – original draft, Supervision, Funding acquisition.

## Declaration of competing interest

The authors declare the following financial interests/personal relationships which may be considered as potential competing interests: Lingfeng Chen reports financial support was provided by National Natural Science Foundation of China. Lingfeng Chen reports financial support was provided by Natural Science Funding of Zhejiang Province. Guang Liang reports financial support was provided by Zhejiang Provincial Key Scientific Project. If there are other authors, they declare that they have no known competing financial interests or personal relationships that could have appeared to influence the work reported in this paper.

## Acknowledgments

This work was supported by the National Natural Science Foundation of China (82103999 to L.C.), Natural Science Funding of Zhejiang Province (LR24H300001 and LQ22H300007 to L.C.), Zhejiang Health Program (YS2022004 to LC), Zhejiang Medical and Health Science Project (2023KY622 to LZ), Zhejiang Provincial Key Scientific Project (2021C03041 to G.L.).

## Appendix A. Supplementary data

Supplementary data to this article can be found online at https://doi.org/10.1016/j.bioorg.2024.107215.

## References

[1] Y. Butt, A. Kurdowska, T.C. Allen, Acute lung injury: a clinical and molecular review, Arch. Pathol. Lab. Med. 140 (4) (2016) 345–350.
[2] M. Chopra, J.S. Reuben, A.C. Sharma, Acute lung injury:apoptosis and signaling mechanisms, Exp. Biol. Med. (Maywood) 234 (4) (2009) 361–371.
[3] L.J. Cross, M.A. Matthay, Biomarkers in acute lung injury: insights into the pathogenesis of acute lung injury, Crit. Care Clin. 27 (2) (2011) 355–377.
[4] R. Malaviya, J.D. Laskin, D.L. Laskin, Anti-TNFalpha therapy in inflammatory lung diseases, Pharmacol. Ther. 180 (2017) 90–98.
[5] O.J. McElvaney, G.F. Curley, S. Rose-John, N.G. McElvaney, Interleukin-6: obstacles to targeting a complex cytokine in critical illness, Lancet Respir. Med. 9 (6) (2021) 643–654.
[6] R.M. Sweeney, M. Griffiths, D. McAuley, Treatment of acute lung injury: current and emerging pharmacological therapies, Semin. Respir. Crit. Care Med. 34 (4) (2013) 487–498.
[7] L. Cheng, Z. Yang, W. Guo, C. Wu, S. Liang, A. Tong, Z. Cao, R.F. Thorne, S.Y. Yang, Y. Yu, Q. Chen, DCLK1 autoinhibition and activation in tumorigenesis, Innovation (camb) 3 (1) (2022) 100191.
[8] F.M. Ferguson, Y. Liu, W. Harshbarger, L. Huang, J. Wang, X. Deng, S.J. Capuzzi, E. N. Muratov, A. Tropsha, S. Muthuswamy, K.D. Westover, N.S. Gray, Synthesis and Structure-Activity Relationships of DCLK1 Kinase Inhibitors Based on a 5,11-Dihydro-6H-benzo[e]pyrimido[5,4-b][1,4]diazepin-6-one Scaffold, J. Med. Chem. 63 (14) (2020) 7817–7826.
[9] F.M. Ferguson, B. Nabet, S. Raghavan, Y. Liu, A.L. Leggett, M. Kuljanin, R. L. Kalekar, A. Yang, S. He, J. Wang, R.W.S. Ng, R. Sulahian, L. Li, E.J. Poulin, L. Huang, J. Koren, N. Dieguez-Martinez, S. Espinosa, Z. Zeng, C.R. Corona, J. D. Vasta, R. Ohi, T. Sim, N.D. Kim, W. Harshbarger, J.M. Lizcano, M.B. Robers, S. Muthaswamy, C.Y. Lin, A.T. Look, K.M. Haigis, J.D. Mancias, B.M. Wolpin, A. J. Aguirre, W.C. Hahn, K.D. Westover, N.S. Gray, Discovery of a selective inhibitor of doublecortin like kinase 1, Nat. Chem. Biol. 16 (6) (2020) 635–643.
[10] Z. Huang, S. Shen, X. Han, W. Li, W. Luo, L. Lin, M. Xu, Y. Wang, W. Huang, G. Wu, G. Liang, Macrophage DCLK1 promotes atherosclerosis via binding to IKKbeta and inducing inflammatory responses, EMBO Mol Med (2023) e17198.
[11] W. Luo, Y. Jin, Y. Jiang, L. Yang, H. Xu, D. Wu, Y. Zhang, L. Yin, Z.A. Khan, G. Liang, Y. Wang, Doublecortin-like kinase 1 activates NF-kappaB to induce inflammatory responses by binding directly to IKKbeta, Cell Death Differ. 30 (5) (2023) 1184–1197.
[12] N. Weygant, D. Qu, W.L. Berry, R. May, P. Chandrakesan, D.B. Owen, S. M. Sureban, N. Ali, R. Janknecht, C.W. Houchen, Small molecule kinase inhibitor LRRK2-IN-1 demonstrates potent activity against colorectal and pancreatic cancer through inhibition of doublecortin-like kinase 1, Mol. Cancer 13 (2014) 103.
[13] O. Patel, W. Dai, M. Mentzel, M.D. Griffin, J. Serindoux, Y. Gay, S. Fischer, S. Sterle, A. Kropp, C.J. Burns, M. Ernst, M. Buchert, I.S. Lucet, Biochemical and Structural Insights into Doublecortin-like Kinase Domain 1, Structure 24 (9) (2016) 1550–1561.
[14] X. Deng, Q. Yang, N. Kwiatkowski, T. Sim, U. McDermott, J.E. Settleman, J.D. Lee, N.S. Gray, Discovery of a benzo[e]pyrimido-[5,4-b][1,4]diazepin-6(11H)-one as a Potent and Selective Inhibitor of Big MAP Kinase 1, ACS Med. Chem. Lett. 2 (3) (2011) 195–200.
[15] Q. Yang, X. Deng, B. Lu, M. Cameron, C. Fearns, M.P. Patricelli, J.R. Yates 3rd, N. S. Gray, J.D. Lee, Pharmacological inhibition of BMK1 suppresses tumor growth through promyelocytic leukemia protein, Cancer Cell 18 (3) (2010) 258–267.
[16] A.V. Galkin, J.S. Melnick, S. Kim, T.L. Hood, N. Li, L. Li, G. Xia, R. Steensma, G. Chopiuk, J. Jiang, Y. Wan, P. Ding, Y. Liu, F. Sun, P.G. Schultz, N.S. Gray, M. Warmuth, Identification of NVP-TAE684, a potent, selective, and efficacious inhibitor of NPM-ALK, PNAS 104 (1) (2007) 270–275.
[17] D.M. Jang, H.J. Lim, H. Hahn, Y. Lee, H.K. Kim, H.S. Kim, Structural Basis of Inhibition of DCLK1 by Ruxolitinib, Int. J. Mol. Sci. 22 (16) (2021).
[18] L. Xing, J. Klug-Mcleod, B. Rai, E.A. Lunney, Kinase hinge binding scaffolds and their hydrogen bond patterns, Bioorg. Med. Chem. 23 (19) (2015) 6520–6527.
[19] A.K. Ghosh, M. Brindisi, Urea Derivatives in Modern Drug Discovery and Medicinal Chemistry, J. Med. Chem. 63 (6) (2020) 2751–2788.
[20] W. Luo, Y. Jin, Y. Jiang, L. Yang, H. Xu, D. Wu, Y. Zhang, L. Yin, Z.A. Khan, G. Liang, Y. Wang, Doublecortin-like kinase 1 activates NF-kappaB to induce inflammatory responses by binding directly to IKKbeta, Cell Death Differ. (2023).
[21] J. Tang, L. Xu, Y. Zeng, F. Gong, Effect of gut microbiota on LPS-induced acute lung injury by regulating the TLR4/NF-kB signaling pathway, Int. Immunopharmacol. 91 (2021) 107272.
[22] J. Ren, D. Su, L. Li, H. Cai, M. Zhang, J. Zhai, M. Li, X. Wu, K. Hu, Anti-inflammatory effects of Aureusidin in LPS-stimulated RAW264.7 macrophages via suppressing NF-kappaB and activating ROS- and MAPKs-dependent Nrf2/HO-1 signaling pathways, Toxicol. Appl. Pharmacol. 387 (2020) 114846.
[23] T.A. Deuel, J.S. Liu, J.C. Corbo, S.Y. Yoo, L.B. Rorke-Adams, C.A. Walsh, Genetic interactions between doublecortin and doublecortin-like kinase in neuronal migration and axon outgrowth, Neuron 49 (1) (2006) 41–53.
[24] C.S. Verissimo, J.J. Molenaar, J. Meerman, J.C. Puigvert, F. Lamers, J. Koster, E. H. Danen, B. van de Water, R. Versteeg, C.P. Fitzsimons, E. Vreugdenhil, Silencing of the microtubule-associated proteins doublecortin-like and doublecortin-like kinase-long induces apoptosis in neuroblastoma cells, Endocr. Relat. Cancer 17 (2) (2010) 399–414.

[25] T. Shu, H.C. Tseng, T. Sapir, P. Stern, Y. Zhou, K. Sanada, A. Fischer, F.M. Coquelle, O. Reiner, L.H. Tsai, Doublecortin-like kinase controls neurogenesis by regulating mitotic spindles and M phase progression, Neuron 49 (1) (2006) 25–39.
[26] M. Mizuguchi, J. Qin, M. Yamada, K. Ikeda, S. Takashima, High expression of doublecortin and KIAA0369 protein in fetal brain suggests their specific role in neuronal migration, Am. J. Pathol. 155 (5) (1999) 1713–1721.
[27] J.S. Liu, C.R. Schubert, X. Fu, F.J. Fourniol, J.K. Jaiswal, A. Houdusse, C.M. Stultz, C.A. Moores, C.A. Walsh, Molecular basis for specific regulation of neuronal kinesin-3 motors by doublecortin family proteins, Mol. Cell 47 (5) (2012) 707–721.
[28] J. Lipka, L.C. Kapitein, J. Jaworski, C.C. Hoogenraad, Microtubule-binding protein doublecortin-like kinase 1 (DCLK1) guides kinesin-3-mediated cargo transport to dendrites, EMBO J. 35 (3) (2016) 302–318.
[29] R. May, S.M. Sureban, S.A. Lightfoot, A.B. Hoskins, D.J. Brackett, R.G. Postier, R. Ramanujam, C.V. Rao, J.H. Wyche, S. Anant, C.W. Houchen, Identification of a novel putative pancreatic stem/progenitor cell marker DCAMKL-1 in normal mouse pancreas, Am. J. Physiol. Gastrointest. Liver Physiol. 299 (2) (2010) G303–G310.
[30] R. May, S.M. Sureban, N. Hoang, T.E. Riehl, S.A. Lightfoot, R. Ramanujam, J. H. Wyche, S. Anant, C.W. Houchen, Doublecortin and CaM kinase-like-1 and leucine-rich-repeat-containing G-protein-coupled receptor mark quiescent and cycling intestinal stem cells, respectively, Stem Cells 27 (10) (2009) 2571–2579.
[31] R. May, T.E. Riehl, C. Hunt, S.M. Sureban, S. Anant, C.W. Houchen, Identification of a novel putative gastrointestinal stem cell and adenoma stem cell marker, doublecortin and CaM kinase-like-1, following radiation injury and in adenomatous polyposis coli/multiple intestinal neoplasia mice, Stem Cells 26 (3) (2008) 630–637.
[32] N. Weygant, D. Qu, R. May, R.M. Tierney, W.L. Berry, L. Zhao, S. Agarwal, P. Chandrakesan, H.R. Chinthalapally, N.T. Murphy, J.D. Li, S.M. Sureban, M. J. Schlosser, J.J. Tomasek, C.W. Houchen, DCLK1 is a broadly dysregulated target against epithelial-mesenchymal transition, focal adhesion, and stemness in clear cell renal carcinoma, Oncotarget 6 (4) (2015) 2193–2205.
[33] S.M. Sureban, R. May, N. Weygant, D. Qu, P. Chandrakesan, E. Bannerman-Menson, N. Ali, P. Pantazis, C.B. Westphalen, T.C. Wang, C.W. Houchen, XMD8-92 inhibits pancreatic tumor xenograft growth via a DCLK1-dependent mechanism, Cancer Lett. 351 (1) (2014) 151–161.
[34] A.D. Jagtap, N.B. Kondekar, A.A. Sadani, J.W. Chern, Ureas: Applications in Drug Design, Curr. Med. Chem. 24 (6) (2017) 622–651.
[35] Y. Zhang, M. Fang, S. Li, H. Xu, J. Ren, L. Tu, B. Zuo, W. Yao, G. Liang, BTApep-TAT peptide inhibits ADP-ribosylation of BORIS to induce DNA damage in cancer, Mol. Cancer 21 (1) (2022) 158.
[36] R. Luo, W. Fu, J. Shao, L. Ma, S. Shuai, Y. Xu, Z. Jiang, Z. Ye, L. Zheng, L. Zheng, J. Yu, Y. Zhang, L. Yin, L. Tu, X. Lv, J. Li, G. Liang, L. Chen, Discovery of a potent and selective allosteric inhibitor targeting the SHP2 tunnel site for RTK-driven cancer treatment, Eur. J. Med. Chem. 253 (2023) 115305.
[37] Z. Liu, L. Chen, P. Yu, Y. Zhang, B. Fang, C. Wu, W. Luo, X. Chen, C. Li, G. Liang, Discovery of 3-(Indol-5-yl)-indazole Derivatives as Novel Myeloid Differentiation Protein 2/Toll-like Receptor 4 Antagonists for Treatment of Acute Lung Injury, J. Med. Chem. 62 (11) (2019) 5453–5469.